TÉCNICO LISBOA

Geometric Analysis of Intracoronary Pressure Curves

Marta Gonçalves Alves

Thesis to obtain the Master of Science Degree in

Biomedical Engineering

Supervisors: Prof. Jorge Filipe Duarte Tiago
Dr. David Cintra Henriques Silva Neves

Examination Committee

Chairperson: Prof. Rita Homem de Gouveia Costanzo Nunes
Supervisor: Prof. Jorge Filipe Duarte Tiago
Members of the Committee: Prof. Marília da Conceição Valente Oliveira Pires

October 2019

Preface

The work presented in this thesis was performed at the Department of Mathematics of Instituto Superior Técnico (Lisbon, Portugal) and at the Digital Angiography and Interventional Cardiology Unit of the cardiology department of Hospital do Espírito Santo - Évora under the CORE project (University of Évora, HESE), during the period February-October 2019, under the supervision of Prof. Jorge Tiago, Dr. David Neves and Prof. Lino Patrício.

Declaration

I declare that this document is an original work of my own authorship and that it fulfills all the requirements of the Code of Conduct and Good Practices of the Universidade de Lisboa.

Abstract

Coronary physiology assessment tests are used to evaluate the physiological severity of angiographically intermediate coronary stenotic lesions. iFR and cFFR are indicators, used in clinical practice, that quantify the ratio between the pressure distal and proximal to a stenosis in predefined zones of the pressure recordings. In this thesis, it is proposed that the severity of a coronary lesion can be related with the geometry of the pressure curve distal to the stenosis. In order to test this hypothesis, a software was developed where pressure recordings were analysed and five new geometric indices were automatically computed in different zones of the cardiac cycle. The commercially available indices, obtained from the device used in clinical practice, were compared to the same emulated indices computed by this new software. The correlation coefficients obtained ($r^2 > 0.97$) in these comparisons suggest a correct automatic identification of cycles and curve time points, validating the method for their automatic detection. The validation of the new physiological indices was performed by comparing them to the iFR, considering a reduced dataset of 39 runs. The indicator that presented the most significant correlation with iFR was Index 7 ($y = 0.77x - 0.506$; $r^2 = 0.2$). These results suggest that the geometrical behaviour of the distal pressure curve is correlated with the severity of coronary lesions, as evaluated with established indices. This finding may have clinical applicability, which should be evaluated in a clinical prospective study.

Keywords

Coronary Physiology; Pressure curve geometry; Instantaneous wave-free ratio; Contrast induced hyperaemia; Myocardial Ischaemia

Resumo

Testes de fisiologia coronária são usados na prática clinica com o objetivo de avaliar o significado fisiológico de lesões coronárias angiograficamente intermédias. O iFR e o cFFR são indicadores que quantificam o rácio entre a pressão distal e a pressão proximal a uma estenose, em zonas predefinidas das curvas de pressão. Nesta dissertação, é proposto que a severidade de uma lesão coronária possa estar relacionada com a geometria da curva de pressão distal à estenose. De forma a testar esta hipótese, foi desenvolvido um software que analisa curvas de pressão, adquiridas no laboratório de cateterismo. Para esta análise, foram calculados cinco índices diferentes em diferentes zonas do ciclo cardíaco. Estes índices, obtidos a partir dos aparelhos usados na prática clínica, foram comparados com uma simulação dos mesmos através do software desenvolvido. Os coeficientes de correlação obtidos ($r^2 > 0.97$) nestas comparações permitem uma validação do método e dos resultados obtidos. Além disso, usando um conjunto de dados reduzido, os novos índices foram comparados com o iFR de forma a avaliar a sua correlação com este índice. O indicador que apresentou uma melhor correlação foi o Índice 7 ($y = 0.77x - 0.506$; $r^2 = 0.2$). Estes resultados sugerem que o comportamento geométrico da curva de pressão distal pode estar relacionado com a severidade da lesão coronária. Estas descobertas poderão vir a ter aplicabilidade clínica, que deverá ser avaliada num estudo clínico prospectivo.

Palavras Chave

Fisiologia Coronária; Geometria da curva de pressão; Instantaneous wave-free ratio; Hiperémia induzida por contraste; Isquémia Miocárdica

Acknowledgments

Apesar de se tratar de um trabalho individual, a realização desta dissertação não teria sido possível sem a influência, direta ou indireta, de várias pessoas que me deram o apoio necessário ao longo destes meses.

Em primeiro lugar, gostaria de agradecer ao Dr. David Neves, por todo o tempo e dedicação que tem aplicado neste projeto desde o início, pelo entusiasmo (com o qual me contagiou), vontade de aprender e de ensinar e especialmente pela enorme disponibilidade que mostrou para me acompanhar. Obrigada ao Prof. Jorge Tiago pela disponibilidade que mostrou para me orientar neste trabalho, em particular na parte mais técnica, na qual se mostrou essencial. Agradeço à Universidade de Évora, na pessoa do Prof. Lino Patrício por se ter disponibilizado para financiar este projeto. Obrigada a todo o staff da Unidade de Angiografia Digital e Cardiologia de Intervenção do serviço de cardiologia do Hospital do Espírito Santo que me acolheram tão bem e se mostraram disponíveis para qualquer dúvida. Não posso deixar de agradecer também à Vanda e à Anniek por terem iniciado este projeto comigo.

Obrigada aos meus amigos. Aos que conheci no Técnico e acompanharam o meu percurso, em particular aos que estiveram nesta fase final e me deram a motivação necessária quando precisei. Aos de Santa Catarina que me acompanham desde sempre (agora sim, já me podem chamar Eng. Tuxa!). Obrigada ao 1211, por me ter ensinado a deixar o mundo um pouco melhor.

Por fim, um grande obrigada à minha família. Obrigada pai e mãe, por darem o vosso melhor para me darem o melhor, pelo valor que dão à minha educação e por dizerem sempre que sim. Obrigada Joana, pela amiga que és, e por teres estado sempre lá para me chamar à razão. Obrigada Tomás, pelos melhores abracinhos e supresinhas que sem dúvida melhoravam a semana. Obrigada avó Matilde e avô António pelos bolinhos e pela lareira que não me deixam esquecer o sítio ao qual pertenço. Obrigada avó Aurora e avô David por serem o exemplo do que é ser boa pessoa. Obrigada tios e primos por todas as maluquices, em especial obrigada aos que me acompanharam mais de perto, tio Cândido, tia Otília e tia Cláudia.

Contents

List of Figures

Acronyms

ACS	Acute Coronary Syndrome
AUC	Area Under the Curve
CABG	Coronary Artery Bypass Grafting
CAD	Coronary Artery Disease
CCS	Chronic Coronary Syndrome
CFR	Coronary Flow Reserve
cFFR	Contrast Fractional Flow Reserve
ECM	Extracellular Matrix
FFR	Fractional Flow Reserve
HESE	Hospital do Espírito Santo de Évora
iFR	Instantaneous Wave Free Ratio
IVUS	Intravascular Ultrasound
LAD	Left Anterior Descending Coronary Artery
LCA	Left Coronary Artery
LCX	Left Circumflex Coronary Artery
NPV	Negative Predictive Value
OCT	Optical Coherence Tomography
OM	Obtuse Marginals
PCI	Percutaneous Coronary Intervention
PDA	Posterior Descending Artery
PLB	Posterolateral Branch
PPV	Positive Predictive Value

RCA Right Coronary Artery

RFR Resting Full-Cycle Ratio

ROC Receiver Operating Characteristic

SCAD Stable Coronary Artery Disease

SMC Smooth Muscle Cell

UADCI Unidade de Angiografia Digital e Cardiologia de Intervenção

WFP Wave-Free Period

1

Introduction

Contents

1.1 Motivation

Due to ageing of the population and its sedentary life habits, hypertension, hyperglycemia and excess of adipose tissue, are becoming more common in today's population. Coronary Artery Disease (CAD) is one of the pathologies that results from the interaction of these risk factors with blood cells and blood vessel wall and is characterized by the accumulation of atherosclerotic plaque in coronary arteries [1]. This disease plays an important role in today's society once it affects a great part of the population, being the leading cause of death worldwide [2].

In order to suit the decision on whether to treat or not and to choose the most appropriate treatment method to apply in each case, it is crucial to have a diagnosis tool that could provide reliable information on the severity of each lesion. Therefore, several diagnosis tools are available in clinical practice, from non-invasive to invasive techniques as is the case of coronary angiography [3, 4].

In most part of the cases, coronary angiography is used to determine the severity of each lesion. However, this method only provides a visual estimation of the lumen diameter reduction of the lesion, not given information on its functional consequences. Thus, angiographically intermediate lesions are often submitted to physiological assessment tests that provide a measurement of the functional significance of the lesion [5].

The gold-standard method for physiological lesion assessment is Fractional Flow Reserve (FFR) [6, 7]. However, the administration of adenosine to induce maximal hyperaemia, needful to measure FFR, is the cause of several side effects [8]. Therefore, some alternatives to FFR have been proposed as is the case of the Instantaneous Wave Free Ratio (iFR) [9].

iFR is measured at rest avoiding the need of hyperaemia and, subsequently, of the administration of adenosine. However, this indicator is commercially restricted to a single software proprietary which limits its extended clinical application. The fact that the contrast agent normally used in clinical practice could induce submaximal hyperaemia, led to the development of an indicator, similar to FFR, that makes use of contrast medium instead of adenosine to induce hyperaemia, the Contrast Fractional Flow Reserve (cFFR) [10, 11]. There are many limitations to the use of cFFR, such as the absence of a dedicated software, the need to record a damped proximal pressure due to contrast injection and the lack of an established protocol for data acquisition.

1.2 Objectives

The main goal of this thesis is to implement a computational algorithm to compute a shape based indicator, able to classify lesion significance from pressure curves under contrast induced hyperaemia. In order to achieve this goal some steps need to be followed as:

- Development of a software able to import pressure data recorded in Hospital do Espírito Santo de Évora (HESE).
- Implementation of filtering methods for the mathematical approximation of pressure data.

- Modeling quantification of lesion significance: volume drop and its interpretation with respect to slope and concavity of both aortic and stenotic pressure curves.
- Numerical algorithm for lesion quantification of generic pressure curves.
- Robustness assessment with respect to iFR and cFFR.
- Statistical analysis.

1.3 Thesis Outline

This thesis is organized in eight chapters.

Chapter 1 presents the motivation and the objectives of this thesis.

In **Chapter 2**, the main concepts for a full understanding of this thesis are explained. A description of the coronary arteries is made with a brief explanation of its anatomy and histology. The normal coronary pressure waveform is described. The main physiopathological mechanisms of CAD and its haemodynamic consequences are described as well as a brief overview of the diagnostic and treatments tools available.

In **Chapter 3** the invasive diagnostic methods used to, in clinical practice, determine the severity of CAD lesions are explained in detail.

In **Chapter 4**, the methodology adopted is presented. This includes the dataset attainment, data treatment process, classification of the different runs, definition of zones in the pressure curve, hyperaemic and resting cycles detection, and the indices calculation. Lastly, the statistical tools used to analyse the results are briefly described.

Chapter 6 and **Chapter 5** include validations of the software and of the new indices developed in this work, respectively.

In **Chapter 7** the results and its discussion of this thesis are presented divided in two sections: the validation of the software and the results for the new indices.

Finally, in **Chapter 8** the conclusions and limitations of this work are exposed.

In **Appendix A** the finite difference schemes used for the calculation of the pressure curves derivatives are displayed. Moreover, Appendix B exhibits additional results regarding Chapter 7.

2

Coronary Artery Disease

Contents

Throughout this chapter, important concepts are defined in order to put into context the scope of this thesis. To fully acknowledge the clinical context, it is important to understand the basics of CAD: pathophysiology, coronary anatomy, histology, and the several treatments available, which are individualized to each patient.

2.1 Coronary Arteries

2.1.1 Anatomy

The coronary arteries supply the myocardium and arise from dilations in the wall of the aorta located superiorly to the aortic semilunar valve, the aortic sinuses. The two main coronary arteries are the Right Coronary Artery (RCA) and the Left Coronary Artery (LCA) arising from the anterior aortic sinus and the left posterior aortic sinus, respectively [12, 13]. In 85% of the population, the RCA is dominant, meaning that it is the artery that supplies the inferior portion of the posterior interventricular septum. In 7 to 8% of the patients, the dominant artery is the LCA. The remaining population presents a codominant system [14]. Figure 2.1 shows the anterior and posterior views of the heart and the coronary arteries.

Left Coronary Artery

The LCA supplies the left atrium, the left ventricle and the interventricular septum. This artery gives rise to two main branches, the Left Circumflex Coronary Artery (LCX) and the Left Anterior Descending Coronary Artery (LAD) [13].

The LCX proceeds along the coronary sulcus to the left and, eventually, fuses with smaller branches of the RCA [13]. The Obtuse Marginals (OM) arise from the LCX and are numbered sequentially [14].

The LAD follows the anterior interventricular sulcus around the pulmonary trunk originating several smaller branches that interconnect with the branches of the posterior interventricular artery [13]. There are two groups of vessels that arise from the LAD, the diagonals and the septal perforators. The diagonals, sequentially numbered, course along and supply the anterior wall of the left ventricle while the septal perforators supply the anterior two-thirds of the interventricular septum [14].

The LCA can also branch into a third vessel, the ramus intermedius which supplies the vascular territory of the diagonal and/or obtuse marginal [14].

Right Coronary Artery

The RCA follows the coronary sulcus and supplies the right atrium, portions of the ventricles and the heart conduction system. Various marginal arteries may arise from the RCA. These arteries distribute blood to the superficial portions of the right ventricle [13].

The Posterior Descending Artery (PDA) arises from the RCA at the crux of the heart running along the posterior portion of the interventricular sulcus toward the apex of the heart. The PDA supplies the posterior interventricular septum and the Posterolateral Branch (PLB). The PLB supplies the posterior and inferior wall of the left ventricle [13, 14].

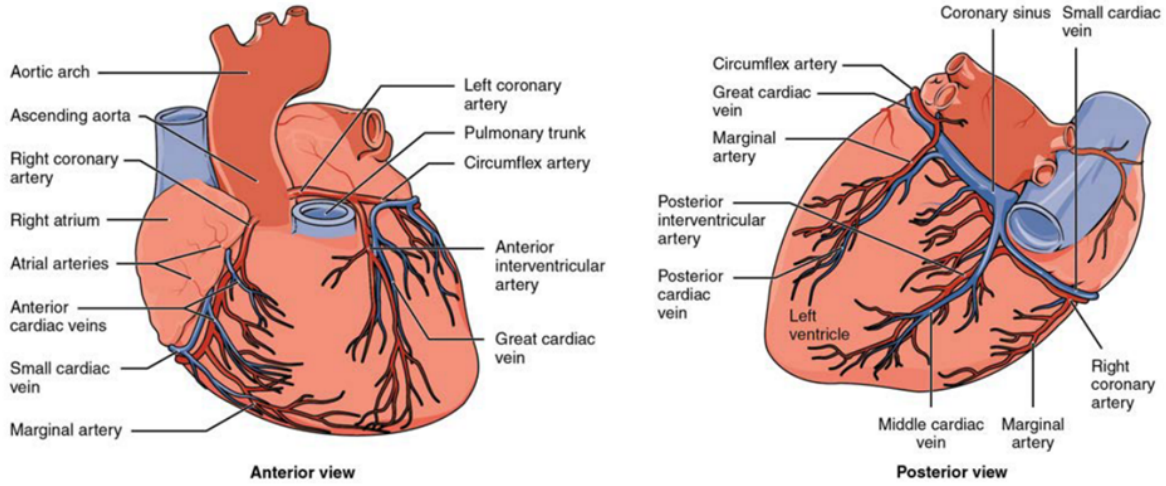

Figure 2.1: Anterior and posterior views of the heart showing the coronary circulation. (From [13])

2.1.2 Histology

The wall of coronary arteries is arranged in three different layers similarly to all other elastic arteries - the intima, the media and the adventitia as shown in Figure 2.2 [12].

The intima, the inner layer, consists mainly of a layer of endothelial cells, and a subendothelial layer of connective tissue. The endothelial cells are attached by occluding junctions and gap junctions forming a selective diffusion barrier between the blood and the other wall layers. Moreover, the endothelium plays an important role in metabolic and endocrine functions being involved in some disease states. Several pathologies seen in elastic arteries develop in the intima. The internal elastic membrane, a fenestrated sheet of elastic tissue, separates the intima from the medial layer [12].

The media consists of a set of smooth muscle and connective tissue layers. The coronary arteries present greater amount of smooth muscle cells and less elastic tissue when compared to other elastic vessels. The external elastic membrane separates the medial layer from the adventitia. Adherent to the outer border of the external elastic membrane are unmyelinated nerve axons that provide neural stimulation to the medial smooth muscle [12].

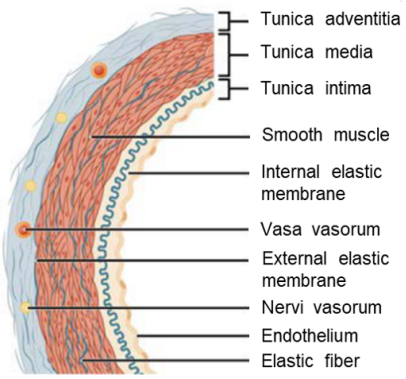

Figure 2.2: Arterial wall, its three layers, the intima, the media and the adventitia and its major constituents (Adapted from [13])

The outer layer of a coronary artery, the adventitia, is formed by fibrous tissue. This layer allows the change in the coronary diameter due to the orientation of its collagen fibers [12].

2.2 Coronary Pressure Waveform

For the purpose of understanding the behaviour of blood in the vascular system, it is important to comprehend the different aspects regarding a healthy and a diseased cardiac cycle, blood flow and blood pressure.

2.2.1 Cardiac Cycle

The sequential relaxations and contractions of the heart provoke a pressure gradient allowing blood to flow through the whole body from areas with higher pressure to zones with lower pressure. These periods of relaxations that cause pressure to decrease and, consequently, blood flow into the chamber in question, are known as diastoles. In parallel, the contraction periods, called systoles, allow blood to flow into circulation [13, 15].

The cardiac cycle can be divided in five stages: atrial systole, isovolumetric ventricular contraction, ventricular ejection, isovolumetric ventricular relaxation and ventricular filling. Aortic, ventricular and atrial pressures during the cardiac cycle are represented in Figure 2.3 [13, 15].

Atrial systole provokes an increase in pressure in the atria pumping blood from the atria into the ventricles. The subsequent contraction of the ventricles - isovolumetric ventricular contraction - causes an arise in ventricular pressure closing the atrioventricular valves. Ventricular ejection happens when ventricular pressure becomes greater than pressure in the pulmonary trunk and in the aorta. Pulmonary and aortic valves (semilunar valves) open pumping blood from the right and left ventricles to the pulmonary trunk and the aorta, respectively. After ventricular ejection, in the begging of ventricular diastole, the

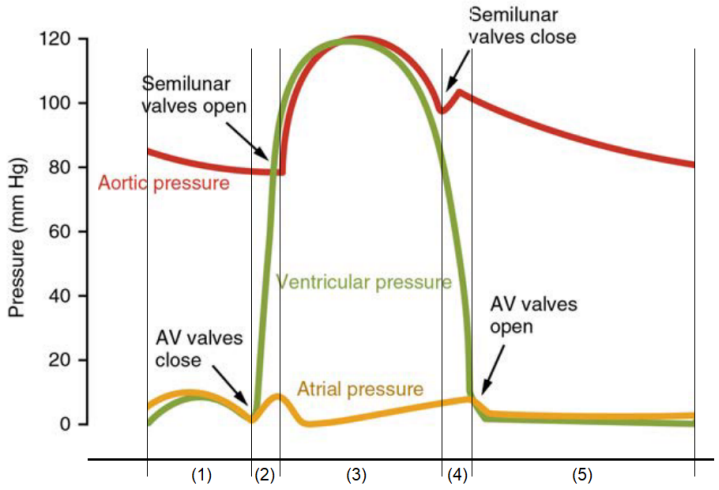

Figure 2.3: Representations of the aortic, ventricular and atrial pressures during the 5 phases of the cardiac cycle - (1) atrial systole, (2) isovolumetric ventricular contraction, (3) ventricular ejection, (4) isovolumetric ventricular relaxation and (5) ventricular filling. Pressure values are expressed in mmHg (From [13])

ventricles relax decreasing the pressure and, consequently, closing the semilunar valves - isovolumetric ventricular relaxation. When ventricular pressure drops below pressure in both, the pulmonary trunk and the aorta, blood tends to flow back toward the heart, causing the closure of the semilunar valves, producing the dicrotic notch. As blood pressure within the ventricles continues to drop below atrial pressure, the atrioventricular valves open and blood flows from the veins to the atria, starting a new cycle. [13, 15].

2.2.2 Blood Flow and Blood Pressure

The relation between blood flow rate, Q, and its pressure gradient, ΔP, in a certain vessel, is given by Poiseulle's equation (Equation 2.1) [15].

$$Q = \frac{\pi \Delta P r^4}{8\eta\lambda} \tag{2.1}$$

where,

r Corresponds to the vessel radius.

η Represents the viscosity of the fluid.

λ Is the length of the vessel.

On the other hand, according to an analogous to Ohm's law in an electrical circuit, flow and pressure gradient can also relate through Equation 2.2 [15].

$$Q = \frac{\Delta P}{R} \tag{2.2}$$

where,

R Corresponds to the resistance.

Substituting Poiseulle's equation in Equation 2.2 (Equation 2.3), it is possible to notice that blood viscosity and the length and radius of the vessel are the variables that influence vascular resistance [15].

$$R = \frac{8\eta\lambda}{\pi r^4} \tag{2.3}$$

In normal conditions, blood viscosity can only slightly fluctuate due to alterations in formed elements and plasma proteins quantity while the length and radius of a vessel change gradually through the vascular system. However, due to its dependence to the fourth power with radius, vascular resistance can abruptly vary with changes in vessel diameter caused by vasodilations or vasoconstrictions [13, 15].

2.2.3 Haemodynamics of Coronary Artery Disease

The presence of a significant stenotic lesion in a vessel produces an increase in blood flow resistance and a decrease in distal pressure, limiting coronary blood flow to the myocardium. When pressure decreases below a certain threshold, myocardial ischemia may happen. As a consequence, the small vessels that regulate local blood flow (resistance vessels) dilate in order to maintain the blood flow and avoid reaching to this state [3].

This reduction in distal pressure is due to energy losses in the stenotic region that create a pressure gradient between proximal and distal arterial regions. These energy losses are caused by viscous friction along the entrance and throat of the lesion and by convective acceleration along the stenosis. As the blood leaves the stenotic region in high velocity, these losses are not recovered due to flow separation and the eddy formation (Figure 2.4). Therefore, in this condition, contrarily on what happens in a healthy vessel (Equation 2.2), the pressure gradient rises with increasing flow velocity, in a quadratic manner, as represented in Figure 2.5 [16].

Some techniques used to assess the severity of stenotic lesions require the administration of vasodilating drugs, such as adenosine (further explanation of these techniques will be provided in Chapter 3). This vasodilating agents minimize microvascular resistance and, thus, maximize blood flow across the stenosis. Healthy vessels and vessels with stenotic lesions respond differently to this hyperaemic stimulus. These different responses are illustrated in Figure 2.6 [17]. In a healthy vessel (Figure 2.6(a)), the vasodilator causes a prominent increase in coronary blood flow, with little divergence of pressures. On the other hand, in the presence of a stenosis (Figure 2.6(b)), the vasodilating agent moderately increases coronary blood flow with a marked increase in the aortic-distal coronary pressure gradient [17].

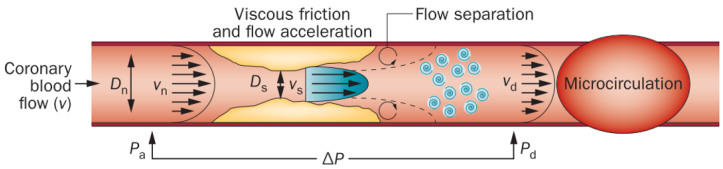

Figure 2.4: Representation of the stenosis flow field. P_a and P_d denote the aortic pressure and the distal pressure, respectively. ΔP represents the gradient of pressure. Flow velocity distal to the stenosis (V_d), proximal velocity (V_n) and stenosis velocity (V_s), normal diameter (D_n), stenosis diameter (D_s) are indicated. (From [16])

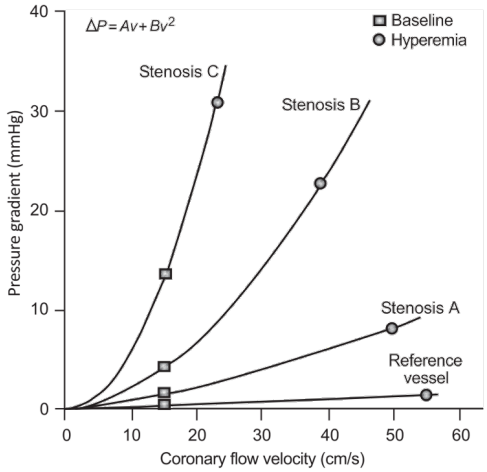

Figure 2.5: Relationship between pressure gradient and coronary flow velocity. This relationship is described by $\Delta P = Av + Bv^2$. Av accounts for the pressure losses caused by viscous friction while Bv^2 represents the losses from the flow separation at the exit. A and B are functions of stenosis geometry and the rheological properties of blood. With increasing stenosis severity (from stenosis A to C), the relationship between the pressure gradient and flow velocity becomes steeper. In a healthy vessel (Reference vessel), this equation reduces to the linear term. (From [16])

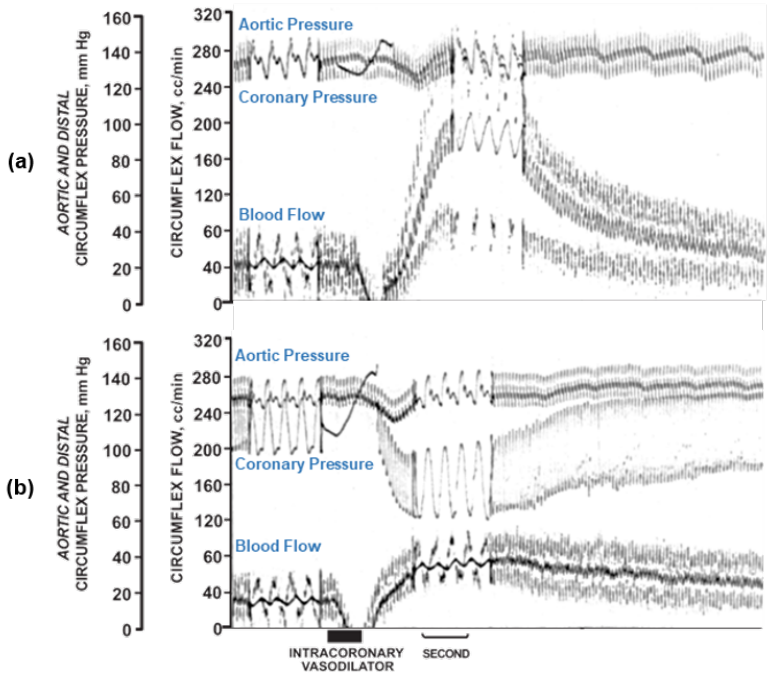

Figure 2.6: Aortic and coronary blood pressure and coronary blood flow tracings from the circumflex coronary artery of a dog. **(a)** Healthy coronary artery. **(b)** Coronary artery with a moderately severe stenosis. Pressure and (Adapted from [18])

2.3 Physiopathology

CAD is a pathological process characterized by atherosclerotic plaque accumulation in coronary arteries causing angina pectoris, myocardial infarction and ischemic heart failure. It is seen as an inflammatory disorder that results from a complex interaction of a large range of risk factors and blood cells [1, 7].

Some of the risk factors are disorders in the metabolism of lipoproteins, substances associated with hypertension, hyperglycemia or derived from the excess of adipose tissue. In the presence of these substances, cells from the arterial endothelium, stimulate the migration of leukocytes from the lumen to the arterial intima. The interaction between the leukocytes, now present in the intima, the endothelial cells and the Smooth Muscle Cells (SMCs) of the tunica media, results in the migration of the SMCs to the tunica intima. In the intima, the SMCs proliferate and initiate the production of Extracellular Matrix (ECM). Lipoproteins bind certain constituents of the ECM prolonging their establishment in the intima and causing them to be prone to modifications. The products of these reactions prolong and proliferate the inflammatory response. Calcification may also occur with the development of the lesion [1].

The distribution of atherosclerotic plaque along the vessel can vary among lesions. Therefore, cross-sectional luminal shape can be divided in two major groups, concentric and eccentric. When the plaque is uniformly distributed along the entire perimeter of the vessel it is called a concentric lumen type. On the other hand, a plaque is known as eccentric when the lesion only occupies a portion of the perimeter leaving a healthy portion [19].

CAD can have long stable periods (Stable Coronary Artery Disease (SCAD)) but can also become unstable at any time, typically due to an acute atherothrombotic event caused by plaque rupture or

erosion. The dynamic nature of the CAD process results in various clinical presentations which can be categorized as either Acute Coronary Syndrome (ACS) or Chronic Coronary Syndrome (CCS) [7].

In order to avoid reaching a state of ischemia and treat the lesion in useful time, a proper detection and lesion significance evaluation using a reliable method is of major importance.

2.4 Diagnosis

As in the majority of other pathologies, an early and accurate diagnosis is a key factor in adequately treating a lesion. Regarding CAD, throughout the years, the development of new technologies permitted a great evolution of the diagnostic tools used in clinical practice, from non-invasive to invasive techniques. The arising of coronary physiology was an importing step for the coronary pathology, since it is now possible to evaluate the physiological significance of each individual lesion [5].

When CAD is suspected, a non-invasive evaluation is normally initiated, in which imaging stress tests (as stress echocardiogram, perfusion scintigraphy/magnetic ressonance, among others) have a predominant role, according to the most recent ESC guidelines. In cases with a very high suspicion or in the event of an ACS, an invasive strategy is usually initiated, with the patient performing a coronary catheterization. During this procedure, various techniques can be applied to evaluate the coronary arteries, and treatment can be immediately performed, if indicated. Coronary angiography, FFR, iFR and cFFR are examples of this techniques that will be discribed in more detail in Chapter 3 [7].

2.5 Treatment

The treatment of CAD aims to alleviate angina symptoms and prevent acute myocardial infarction or premature death.

On one hand, medical therapy consists of a prescription of drugs that mainly control angina and prevent or reverse plaque progression. On the other hand, invasive strategies as Coronary Artery Bypass Grafting (CABG) and Percutaneous Coronary Intervention (PCI) focus on reestablishing adequate blood supply to the damaged myocardial zones due to severe coronary occlusion [20]

PCI is a non-surgical procedure commonly performed via the femoral or the radial artery and consists of placing a stent in the impaired artery in order to restore normal blood flow in that territory [21]. CABG is a surgical procedure where a piece of a healthy blood vessel from other part of the vascular system is connected below and above the narrowed artery, bypassing the injured coronary arteries [22].

According to the 2018 ESC/EACTS Guidelines on myocardial revascularization [23], the choice of the revascularization strategy , CABG or PCI, in patients with SCAD depends on anatomical (lesion distribution and characteristics) and clinical (age, presence of diabetes, etc) factors, which may be assessed with dedicated scores, like the SYNTAX score. Therefore, the diagnostic assessment of patients with CAD is crucial to identify patients and select which lesions would benefit from myocardial revascularization and how it should be performed [23].

3

State of the Art

Contents

Invasive strategies are usually used in clinical practice when there is a high suspicion of coronary artery disease, such as in the presence of typical anginal chest pain, evidence of extensive ischaemia on non-invasive tests or in the event of an ACS, as referred in Chapter 2. In the present chapter, some of these techniques are described reinforcing the importance of an accurate detection of the disease, as well as the detailed determination of the severity and exact location of each lesion in order to adequately treat each particular case.

3.1 Coronary Angiography

Angiography is an imaging technique that permits the visualization of blood vessels using radiation. After the first angiography was performed by Egas Moniz in 1929 [24], with the aim of visualizing the brain vessels, this technique is being widely used to visualize other vessels, for instance, coronary arteries.

Coronary angiography is an x-ray analysis of the cardiovascular system which allows the visualization of the coronary arteries and its branches. The coronaries can be accessed either through the radial or femoral arteries. Usually, the radial access is preferred as it is smaller, more superficial and thinner than the femoral artery making it easier to achieve hemostasis after the procedure [25].

In order to perform a coronary angiography, the operator introduces the angiographic catheter on the chosen artery and conducts it through the artery to the aortic root. A contrast agent is injected in an attempt to visualize the coronary tree as well as its possible lesions. The stenosis severity is then estimated comparing, visually, the percentage of lumen reduction between the narrowed segment and an apparently normal adjacent segment, seen in the worst x-ray projection [26].

The fact that, with this method, stenosis severity determination is based on a visual estimation introduces some uncertainty in stenosis severity quantification. Firstly, being a two-dimensional projection of a three-dimensional structure, the angiogram provides few intraluminal details that could permit the characterization of a plaque. Secondly, the clear distinction between a healthy and a diseased vessel can be biased by the existence of diffused CAD which may be difficult to detect in an angiogram. Furthermore, the assumption that the arterial lumen is circular and the eccentric shape of places impedes the quantification of the obstruction degree of a lesion. All these factors contribute to a high variation of readings making angiography a not reliable method to direct coronary revascularization, specially on intermediate level lesions [3].

In order to avoid this uncertain diagnosis, there are alternatives to angiography. Some of those techniques, as Intravascular Ultrasound (IVUS) and Optical Coherence Tomography (OCT), provide a visualization of the arterial lumen and wall allowing the measurement of the vessel anatomy and lesion morphology [3].

The techniques mentioned in this section provide the visualization of the vessel, either allowing the observation of a longitudinal projection or the cross-section of the vessel conferring an anatomic measurement of the lesion. However, the relationship between this anatomic measurements and the presence or absence of myocardial ischemia is complex and, in many cases, angiography does not give a clear perception of the consequences that each lesion has on blood flow. Advances in technology en-

abled the assessment of coronary physiology in the cath lab, facilitating a measurement of the functional significance of a lesion. In this direction, Coronary Flow Reserve (CFR) and, in more recent studies, FFR, iFR and cFFR were developed having demonstrated physiologic accuracy and prognostic value for the assessment of coronary artery disease. These tools allow cardiologists to make decisions based on objective findings [5]. In the following sections, these coronary physiology assessment tools will be analysed in detail.

3.2 Coronary Flow Reserve

The first quantitative haemodynamic relationship between lumen reduction and CFR was purposed by Lance Gould *et al.* [27] in 1974.

As consequence of the presence of coronary stenosis or other conditions, the resistance vessels dilate in order to maintain coronary blood flow required by the myocardial oxygen demands. This mechanism prevents the reduction of the resting coronary flow in cases with lumen diameter reduction of up to 90%. However, this autoregulation process leads to a gradual reduction of the coronary vasodilatory reserve. Therefore, the maximal coronary blood flow is affected by lesions with a lumen diameter reduction starting in 50% [15, 16, 28].

The CFR expresses this vasodilator capacity of the coronary vessels in response to an increase in the oxygen demands [27]. CFR is measured as the ratio between the maximal coronary blood flow and the resting coronary blood flow (Equation 3.1) [15].

$$CFR = \frac{Q_{max}}{Q_{rest}} \tag{3.1}$$

where,

Q_{max} Corresponds to the maximal coronary blood flow.

Q_{rest} Represents the coronary blood flow at rest.

Figure 3.1 illustrates the relationship between coronary blood flow and pressure in the presence of a stenosis, during hyperaemia and in normal conditions. Basal flow is mainly influenced by the autoregulatory response of coronary arteries. However, there are physiological and pathophysiological factors, independent of stenosis severity, that also affect it. The dependence of this ratio on basal flow condition and, consequently, its sensitivity to changes on basal flow, constitutes an important limitation of CFR [16]. This limitation, together with some technical issues, led to the introduction of other means of functional lesion severity measurement such as FFR, developed by Pijls and De Bruyne [6, 28].

3.3 Fractional Flow Reserve

FFR is defined as the ratio between the maximal myocardial flow measured in the stenotic territory and the theoretical maximal blood flow in the same territory in the absence of stenosis [6].

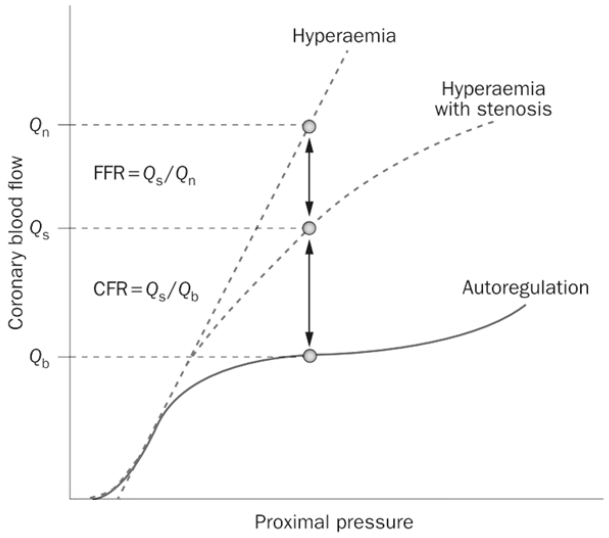

Figure 3.1: Relationship between coronary blood pressure and flow during hyperaemia in the presence and in the absence of a stenosis (dashed lines) and in the absence of a hyperaemic stimulus in the presence of stenosis (solid line). Q_s is the hyperaemic flow in the absence of a stenosis. Q_s is the hyperaemic flow in the presence of a stenosis. Q_b is the basal flow. (Adapted from [16]).

In the presence of a stenosis, the pressure gradient is related to coronary blood flow in a quadratic manner, as depicted in Figure 2.5. However, during maximal dilatation of the coronary vascular bed, energy losses are minimized and coronary perfusion pressure and flow are assumed to be linearly proportional, as illustrated in Figure 3.1 [16].

Therefore, under these conditions, FFR can be computed as the ratio between the coronary pressure before the stenosis (aortic pressure) and the coronary pressure distal to the stenosis (Equation 3.2).

$$FFR = \frac{P_d}{P_a} \text{ , at maximal hyperaemia} \tag{3.2}$$

where,

P_d Corresponds to distal pressure.

P_a Represents the aortic pressure.

The fact that both distal coronary pressure and aortic coronary pressure are measured during maximal vasodilation, makes FFR independent of factors that influence basal flow conditions [16].

A state of maximum coronary vasodilation, meaning maximal blood flow in the coronaries can be reached through different stimuli. A response to coronary occlusion - the reactive hyperaemic response is one example of these stimuli. Despite being the most potent stimulus to hyperaemia, it presents some limitations. Firstly, in some cases, its effect might be submaximal and, secondly, the left main trunk cannot be occluded for 60s. These observations led to the use of vasodilating drugs to the purpose of achieving maximal hyperaemia [15, 29].

Despite presenting some limitations, mainly due to the side effects produced by the vasodilating drugs needed to induce hyperaemia, according to the European Society of Cardiology 2019 guidelines [7], FFR should be available and considered during a coronary angiography. This would allow

the confirmation of the diagnosis of CAD in patients with uncertain diagnosis on non-invasive testing. Lesions presenting a FFR value inferior or equal to 0.8, considered to be high risk lesions, should then be treated. Thus, FFR is used as a complement to coronary angiography especially in patients with coronary stenoses of 50-90% or in cases of multi-vessel disease due to the frequent mismatch between the angiographic and hemodynamic severities of coronary stenoses [7].

3.3.1 Vasodilating Drugs

Administration of intravenous adenosine is currently the gold-standard method to achieve of maximum coronary hyperaemia, being the best combination between hyperaemia and side effects. Intravenous adenosine enables a reproducible and maximum arteriolar vasodilatation long enough to make a reliable pullback recording along a diseased artery. These pullback recording allow a local FFR measurement in patients with multivessel disease or multiple abnormalities along a coronary artery. Nevertheless, the administration of intravenous adenosine is time-consuming and relatively costly [28, 30].

Other option is the intracoronary administration of adenosine. However this technique presents a very short-lasting hypereamia which is insufficient to make a pressure pullback recording. Moreover, in order to achieve hypereamia values comparable to intravascular adenosine, there is a higher risk of atrio-ventricular block.

Other alternatives to adenosine also present some limitations. The use of intracoronary papaverine has an associated risk of polymorphic ventricular tachycardia. The administration of intracoronary sodium nitroprusside can induce severe hypotension [28]. Recent studies have shown that the peripheral infusion of regadenoson has less side effects when compared to intracoronary adenosine [8].

Due the limitations introduced in the measurement of FFR by the need of hyperaemia and, in an attempt to avoid this problem, some investigators started to think the possibility of indexes that could be measured at a resting state.

3.4 Instantaneous Wave-Free Ratio

In an attempt to avoid the need of hyperaemia in coronary disease risk assessment, investigators [9] studied the possibility of existing a time period that could be identified from the resting pressure waveform when the resistance would be naturally constant and minimized. This way avoiding the need of hyperaemia, saving time and reducing costs and side effects [28].

In order to identify this time period in the cardiac cycle, a wave-intensity analysis was performed according to the methodology described by Davies *et al.* [31]. This analysis enabled the identification of a Wave-Free Period (WFP) after diastole when no new waves are generated and where intracoronary resistance remained minimized and stable (Figure 3.2) [9].

The onset of diastole was identified from the dicrotic notch, and the diastolic WFP was described as the period beginning 25% of the way into diastole and ending 5 ms before the end of diastole [9].

Therefore, a resting index was proposed, iFR, calculated as the ratio between the mean pressure

distal to the stenosis during the diastolic WFP and the mean aortic pressure during the same period (Equation 3.3) [9].

$$iFR = \frac{P_d}{P_a} \text{ , during diastolic wave-free period} \tag{3.3}$$

where,

P_d Corresponds to distal pressure.

P_a Represents the aortic pressure.

Sen *et al.* [9] concluded that the resistance values are similar during the diastolic WFP at rest and during adenosine mediated FFR and that the iFR correlates closely with FFR ($r^2 = 0.90$). In the ADVISE II study [32], the authors suggest that 0.89 would be a optimal iFR cutoff value, meaning that lesions in iFR values under or equal 0.89 should be considered high risk lesions and should be treated.

Some studies have been testing the existence of a WFP and the correlation between iFR and FFR claimed in the ADVISE study [9]. In the VERIFY study [33], it is suggested that the diagnostic accuracy of iFR was low using a cutoff value of either 0.80 or 0.83 - 60% and 68%, respectively. The authors also advocate that iFR changes during adenosine-induced hyperaemia, contradicting the definition of iFR, which is said to be independent of hyperaemia. Finally, the resistance in the diastolic WFP is said to be generally 50% to 100% higher than the average resistance over the complete cardiac cycle during hyperaemia, contrary to what is proposed by Sen *et al.* [9]. However, the software used in this study to estimate iFR was a non-proprietary software which may represent a limitation [28].

In the RESOLVE study [34], the authors conclude that a hybrid approach where FFR is used only in cases where iFR is in the gray area would avoid the use of hyperaemia in 65% of the lesions, considering a correlation of $\geq$90% with an FFR cutoff $\geq$0.80.

The DEFINE-FLAIR [35] and the iFR-SWEDEHEART [36] trials tested the hypothesis, proposed by Sen *et al.* [9], that the discrepancies between iFR and FFR could not impact on clinical outcomes. In these multi-centered and randomized studies, 4529 patients (2037 in the iFR-SWEDEHEART [36] and 2492 in the DEFINE-FLAIR [35]), who had an indication for physiologically guided assessment of a coronary lesion (with 40 to 70% [35] or 80% [36] stenosis on visual examination), were randomly assigned to undergo revascularization guided by either iFR or FFR. Both studies concluded that revascularization guided by iFR was non-inferior to revascularization guided by FFR, with respect to the risk of major adverse cardiac events at 1 year. Regarding the rate of adverse procedural signs and symptoms and the procedural time, both were shorter with iFR than with FFR [35,36]. However, these studies present some limitations, such as the short follow-up and the relatively low risk profile of the enrolled populations [28].

In 2017, van't Veer *et al.* [37] analysed and compared various diastolic resting indexes, concluding that all of them could be used interchangeably and, thus, that all cutoff values, clinical recommendations and guidelines used for iFR are directly applicable to the diastolic indices in question. Moreover, their data also indicates that a particular WFP does not exist [37]. Therefore, and as an example, in 2018 Svanerud *et al.* [38] proposed the validation of utilization of Resting Full-Cycle Ratio (RFR) as a novel non-hyperemic index of coronary stenosis severity. RFR is computed as the lowest ratio between distal

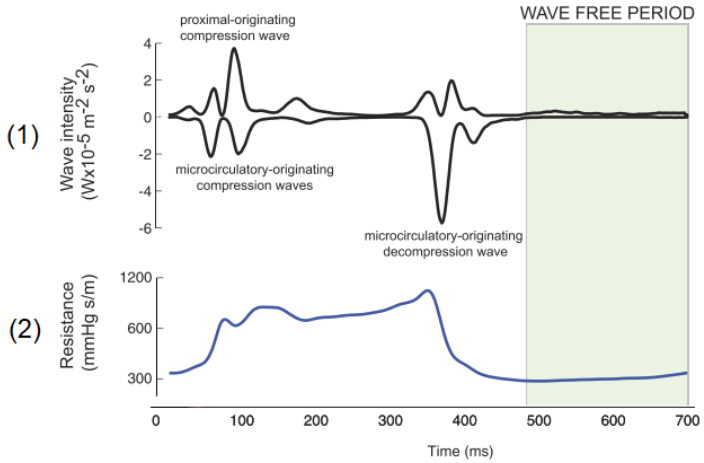

Figure 3.2: Identification of the Wave-Free Period. (1) Wave intensity, expressed in $W10^{-5}m^{-2}s^{-2}$, demonstrating the different waves generated during the cardiac cycle. Wave-Free Period (shaded) where no new waves are generated corresponding to a period of minimal and constant Resistance (2) expressed in $mmHg\ s\ m^{-1}$. (Adapted from [9]).

and aortic coronary pressure during a cardiac cycle (Equation 3.4). In line with van't Veer *et al.* study conclusions, the cutoff value for RFR is the same as the one used for iFR, 0.89 [38].

$$RFR = min(\frac{P_d}{P_a}) \text{ , during a cardiac cycle} \tag{3.4}$$

where,

P_d Corresponds to distal pressure.

P_a Represents the aortic pressure.

3.5 Contrast Fractional Flow Reserve

In 1959, S. Guzman and J. West [10] reported that the intracoronary administration of contrast agents increased coronary blood flow and that this increase was a consequence of a reduction on coronary vascular resistance. Later, in 2003, De Bruyne *et al.* [39] compared the hyperaemic effect of the administration of different drugs including adenosine, papaverine and contrast medium (iohexol). They concluded that intracoronary administration of contrast medium produced a hyperaemic effect, even that significantly weaker and shorter than other stimuli [39].

More recently, in 2015, Leone *et al.* [11] proposed cFFR, a new index computed as the ratio between distal coronary pressure and aortic pressure measured after achievement of hyperaemia using contrast medium. In this study, the RINASCI study, the authors tested the hypothesis that the submaximal hyperaemia induced by a intracoronary injection of conventional non-ionic contrast medium could be sufficient for the assessment of the physiological severity of stenosis [11].

Leone *et al.* [11] observed a good correlation between cFFR and FFR ($r^2 = 0.88$) concluding that, considering a cutoff value of $\geq$0.83, this new index could allow limiting the use of adenosine to cases in the gray zone - cFFR between 0.84 and 0.87 [11].

Other studies [40, 41] have been produced with the aim of correlating cFFR with FFR, concluding that cFFR is more accurate predicting FFR when comparing to iFR or other resting indexes.

cFFR appears to be safe, cheap and easily applicable in the clinical practice. Therefore, the choice of a hybrid approach, combining cFFR with FFR, would maximize accuracy while sparing time and costs and avoiding the side effects caused by the use of adenosine [11].

4

Methods

Contents

In order to fulfill the previously described objectives of this thesis, a strict and well defined methodology was undertaken. In this chapter, the consecutive steps of those methods will be described in detail. Firstly, the medical protocol used for the recording of the pressure curves is explained. Secondly, the data treatment process is described, including the process of data import and data filtering. Subsequently, the run identification process is shown. The zones important to the analysis of both distal and proximal pressure curves are defined and illustrated. Finally, a description of the different indices computed in this work is given.

4.1 Data Acquisition

The dataset analysed in this work was acquired by the multidisciplinary team (cardiologists, cardiopneumology and radiology technicians and nursing staff) of the Unidade de Angiografia Digital e Cardiologia de Intervenção (UADCI), the catheterization laboratory (cath lab) of HESE. In the HESE cath lab, there are two different sets of hardware and software available, developed by two different companies, that collect intracoronary pressure recordings and measure the severity of stenoses present in coronary arteries. These machines are the Quantien™ console from Abbott compatible with the PressureWire™ X pressure guide wire and the CORE™ console from Philips that uses the Volcano Verrata® Plus pressure guide wire to measure intracoronary pressure.

4.1.1 Patient Selection

Lesions with 50 to 70% of lumen diameter reduction are considered as angiographically intermediate. In this case, angiogram does not give clear information on the severity of the lesion and, subsequently, its impact on myocardial perfusion. Therefore, when clinically indicated, patients presenting lesions within this range of severity were submitted to a physiology assessment test in order to clarify whether that lesion would benefit from a revascularization helping the cardiologist in that decision.

From 2015 to 2019, 122 patients with intermediate angiographic lesions were submitted to a physiological severity assessment. The dataset obtained from this medical exams forms a total of 769 runs - 324 iFR runs, 88 RFR runs, 42 FFR runs and 179 cFFR runs (the remaining 136 were excluded from analysis as will be explained in Section 4.3).

4.1.2 Medical Procedure

After performing an angiography and deciding to proceed to a physiology assessment, the UADCI team follows the procedure described below.

The procedure initiates with the equalization of pressures with the catheter filled with blood (after allowing backflow of blood in the catheter). Special care is taken in order to avoid damping of pressures, with the equalization taking place in the ascending aorta if necessary. An intracoronary injection of nitrates (1-3mg of Isosorbide dinitrate) is administered in order to prevent coronary vasospasm and produce a vasodilation of larger coronary arteries [42]. The pressure wire is then advanced until the

pressure sensor is two to three vessel diameter lengths distally to the lesion, and the iFR and Pd/Pa (ratio between mean distal and aortic pressure recordings) values are registered. During equalization and measurement, the pointing needle is removed from the ”Y” connector. During these steps the catheter is filled with blood.

cFFR is then computed in cases where the iFR and Pd/Pa values are inconclusive to decide about a lesions' severity and in cases where the patient does not present any contraindication on the use of a contrast agent as is the case of renal insufficiency or a ostial lesion that hampers the contrast of reproducibly entering the coronary artery. A standard full contrast injection is administered intracoronarily by the ACIST CVi^{TM} contrast delivery system (6 ml at 4 ml/s for the LCA and 5 ml at 3 ml/s for the RCA, with a maximal pressure of 300 psi), five beats after the start of the recording. The recording is then discontinued approximately 15 seconds after the injection of contrast.

In the event that cFFR is also inconclusive, FFR is calculated. The recording of distal and aortic pressures is initiated before the intravenous perfusion of adenosine. A good peripheral (median antecubital) vein, or a central (femoral) vein is used for the continuous adenosine perfusion (140 μg/Kg/min).

After obtaining the desired indices, a pullback run is performed in order to locate the lesion that may be causing the difference in pressure. Additionally, a drift check run is performed to verify the equalization of both aortic and distal pressure curves. A maximum drift of $\pm$0.02 Pd/Pa ratio is allowed.

Depending on the machine used to perform the exam, different run types and indices can be measured. Abbott's software enables the recording of a dedicated Pd/Pa run. In this software iFR is not measured, since it is intellectual property of Philips. Instead, RFR, which measures the lowest Pd/Pa during a full cardiac cycle, is computed. Despite this, the interpretation of these two indices by the medical team is similar. FFR and cFFR are recorded in a similar way in both machines, although there is no dedicated software for cFFR analysis in any of them.

4.2 Data Processing

Once the files were exported from the proprietor hardware, data were analysed using Python^{TM}(Python Software Foundation, https://www.python.org/).

4.2.1 Importing the Data

After being recorded in the cath lab, the pressure data is imported to Python. Here, the different columns present in the files are separated. The data files are organized differently and exhibit different information depending on the software used to record the pressure curves. Despite that, both data acquisition software contain the recording times and respective aortic pressure (Pa), distal pressure (Pd). Once files from Philips' software contain all runs related to a certain patient, these runs are separated. On the other hand, files from the software from Abbott are already separated run by run. Posteriorly, the information of each run is imported to a *dictionary*, a data type built into Python.

4.2.2 Data regularization

With the aim of studying the behaviour of the pressure curve geometrical features, and due to the presence of noise inherent to the recording of a biological signal, the blood pressure recordings were filtered using a regularization technique, which we call regularization method 1.

This method reduces the noise while maintaining the shape and height of waveform peaks, contrarily to a typical moving average fitting that reduces the function value at local maxima. Other authors have already used the regularization method 1 with the aim of smoothing blood pressure recordings as is the case of the work developed by Davies *et al.* [31].

Subsequently, three geometric measures, A, B and C were computed from the regularized data.

4.2.3 Geometric Measures

In order to define most part of the zones of interest in this work, it was necessary to compute distal and/or aortic pressure curve geometric measures which we identify as A, B and C.

4.3 Run Identification

Once the regularization is achieved, the identification of each run is required given that each run type present different characteristic features. Subsequently each group of run will follow a different approach.

As depicted in Figure 4.1, the input files can include three types of runs - iFR runs, FFR runs and cFFR runs (RFR runs where classified as iFR runs). Each of these run types has specific characteristics that enables is classification.

iFR runs were identified as lasting less than 15 seconds (Figure 4.1(a)). On the other hand, runs lasting more than 15 seconds and that exhibited an injection artifact - artifact caused by the intracoronary injection of a contrast medium - were considered to be cFFR runs (Figure 4.1(c)). Runs longer than 1 minute were identified as FFR runs (Figure 4.1(b)). Lastly, runs that did not fit any of the above mentioned parameters were classified as unidentified.

Previously to run identification, some runs were excluded from analysis once they were not considered relevant in this work. Figure 4.1 exhibits three examples of these runs that could have derived from different situations. Pullback runs, as present in Figure 4.1(d), enable the operator to confirm that both distal and aortic pressure sensors were equalized. Furthermore, a drift check run is depicted in Figure 4.1(e). These runs are recorded in order to verify the influence of the fluid filing catheter on pressure recordings and to validate the previous measurements. Finally, there are runs in which the presence of several artifacts impeded their analysis and, consequently, these runs were excluded from this work (Figure 4.1(f)). These artifacts could be caused by an unstable catheter position, whipping of the pressure wire sensor, or other technical issues.

4.4 Definition of Zones

In order to study the pressure recordings and extract information about the relationship between its geometrical behaviour and the severity of the lesion in question, it is crucial to define zones of interest that will be useful to the calculation of new indices.

4.4.1 Cardiac Cycle

First of all, and more important, the beginning and the end of each cardiac cycle in the distal pressure were defined. The beginning of each cardiac cycle was defined using the geometric measure C of the pressure curve, between the minimum of the previous cycle and the maximum of the cycle in question. The end of each cardiac cycle matches the beginning of the previous cycle. These points are represented in Figure 4.2.

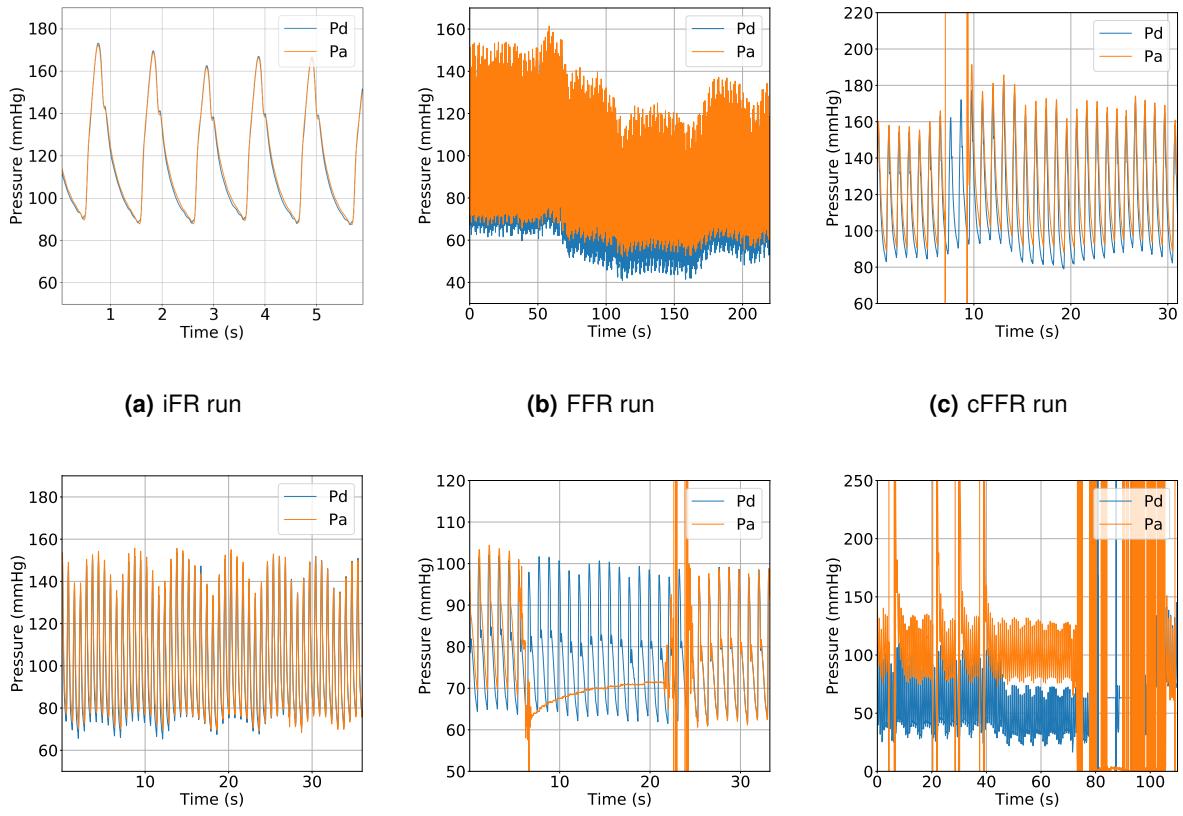

(a) iFR run **(b)** FFR run **(c)** cFFR run

(d) Pullback run **(e)** Drift check run **(f)** Error run

Figure 4.1: Identification of the different run types considered in this work (top panel) and examples of runs excluded from analysis (bottom panel). Distal pressure curve (Pd) in blue. Aortic pressure curve (Pa) in orange. Pressure expressed in mmHg and time expressed in seconds.

4.4.2 Dicrotic Notch

The identification of the dicrotic notch is crucial for the delineation of other zones in the pressure curve, as is the case of the WFP.

The closure of the aortic valve produces the dicrotic notch, a true upstroke in the waveform, in the arterial pressure curve indicating the end of blood ejection. However, due to pathophysiological alterations and/or normal physiological variability in vascular properties, dicrotic notches often vary substantially in terms of their positions and morphologies, degenerating, in some cases to an *incisura* which is a simple inflection in the waveform [43, 44].

Based on previous works from different authors [43, 44], in this work, a different dicrotic notch detection algorithm was developed by analysing the pressure waveform. First of all, for each cycle, the point corresponding to the dicrotic notch was found, using the geometric measure C.

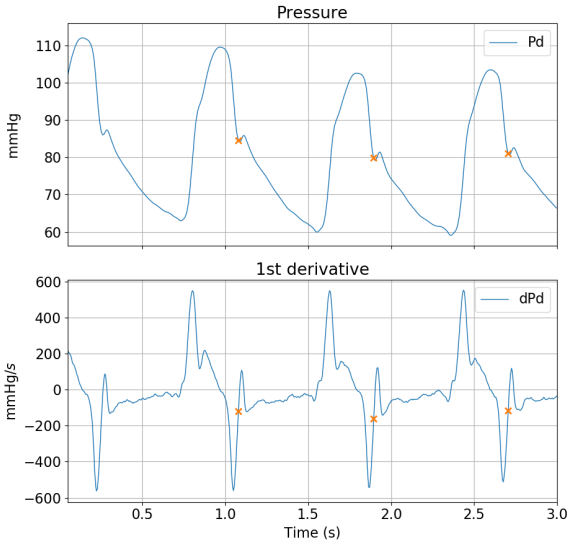

Figure 4.3: Identification of the dicrotic notch. Distal pressure curve (Pd) Dicrotic notch **(a)**. Pressure expressed in mmHg and time expressed in seconds.

4.4.3 Wave-Free Period

Accordingly to the ADVISE study [9], iFR is the ratio between the mean distal pressure and the mean aortic pressure, both calculated during the WFP. Sen at al. [9] describe the WFP as the period starting

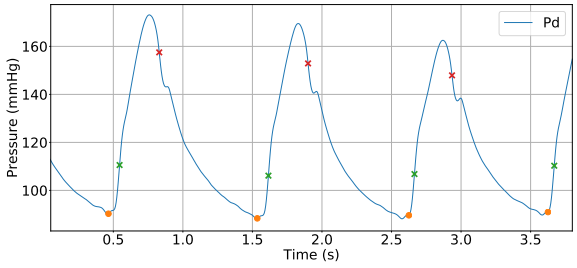

Figure 4.2: Identification of the limits of each cardiac cycle. Distal pressure curve (Pd). Pressure expressed in mmHg and time expressed in seconds.

in 25% of the diastole and ending 5 ms before the end of the diastole. The diastole is then defined as the time interval from the dicrotic notch to the end of the cycle.

In this thesis, for each cycle, the diastole was defined as the period between the dicrotic notch and the beginning of the following cycle, discarding the small oscillations that could occur in the final 30% of the cycle. Therefore, the beginning of the WFP was identified as the point 25% after the beginning of the diastole and its end coincident to the end of the diastole (Figure 4.4).

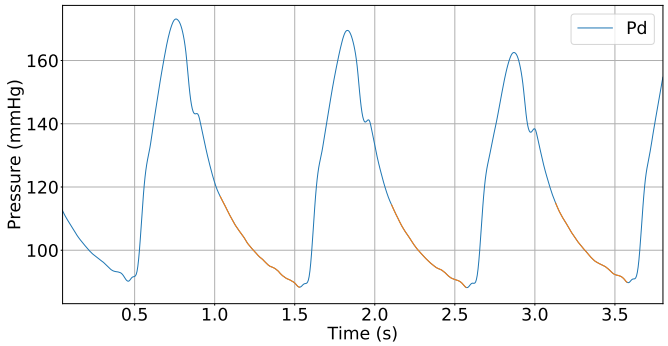

Figure 4.4: Wave-free period identification. Distal pressure curve (Pd) in blue. Wave-free period in orange. Pressure expressed in mmHg and time expressed in seconds.

4.4.4 Other Zones

Additionally to the delineation of the WFP, other zones of interest were defined with the aim of studying the geometrical behaviour of the intracoronary pressure curves during these periods. Therefore, three zones were defined and named as Period 1, Period 2 and Period 3.

4.4.4.1 Period 1

The Period 1 was defined as in (Figure 4.5).

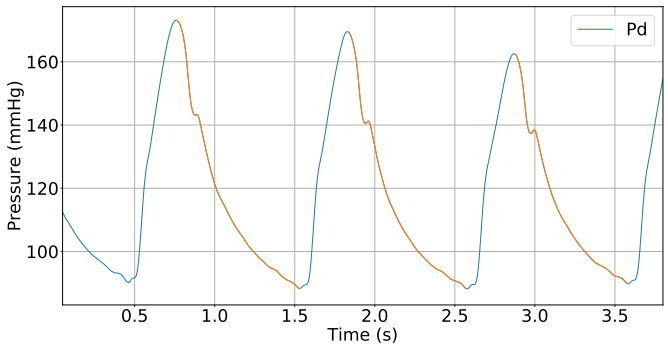

Figure 4.5: Identification of the Period 1. Distal pressure curve (Pd) in blue. Period 1 in orange. Pressure expressed in mmHg and time expressed in seconds.

4.4.4.2 Period 2

For each cycle, a zone named Period 2 was using the geometric measure C of the distal pressure curve and finishing at the dicrotic notch.

In cases where this interval was smaller than the necessary to perform an analysis, i.e. lasting less than 5 recording points, more points prior to this minimum were considered making a total of 5 points.

4.4.4.3 Period 3

In order to better study the behaviour of the pressure waveform during the diastole, a Period 3 was identified in the pressure curve. This zone has its beginning in a point found using the geometric measure C of the distal pressure, after the dicrotic notch and its end coincident with the end of the diastole.

4.5 Resting and Hyperaemia Detection

Regarding cFFR runs, it is crucial to delimit two time intervals - the resting period and the hyperaemic period. The resting period was defined as the period before the intracoronary injection of contrast medium that would induce hyperaemia. The hyperaemic period was considered to be the time interval where the coronaries are under the effect of the hyperaemic agent, in this case, of the contrast agent.

4.5.1 Injection Artifact

The injection of contrast medium in the coronaries causes an abruptly change in aortic pressure, here called injection artifact. This injection artifact was identified as the zone where aortic pressure is below 40 Hgmm (this value was obtained by observation of the behaviour of the available dataset). In runs with more than one injection artifact, and with a distance between them of more than approximately 20 cycles, the injection artifact considered was the first one, thus the rest zone was considered before this first artifact and the hyperaemic zone will be considered between the two injection artifacts (Figure 4.6).

With the purpose of accurately defining the injection zone, its initial and final points were adjusted in a way that both had their pressure values in the range between the minimal and the maximal pressure before and after of the injection zone, respectively.

4.5.2 Resting Cycles

The resting zone was defined as the zone between the beginning of the pressure recording and the beginning of the injection zone. Within this zone, the three resting cycles that corresponded to the three cycles presenting more stability, meaning that the mean difference between their consecutive peaks was minimum, were delimited. These peaks location was obtained using the Python function *find_peaks* from the signal processing toolbox (Figure 4.6). In cases where the recording had less than three cycles before the injection zone, all cycles in the resting zone were considered to be resting cycles. In an extreme case of a pressure recording not having a single entire cycle before injection, this would impede the analysis of the run in question.

4.5.3 Hyperaemic Cycles

The hyperaemic zone was identified as the zone starting four cycles from the end of the injection zone and ending twenty cycles from the end of the injection zone. The three hyperaemic cycles were defined as the three consecutive cycles, within the hyperaemic zone, which presented the maximum hyperaemia, in other words, that presented the maximal difference between mean aortic pressure and mean distal pressure (Figure 4.6). The existence of less than one cycle after the injection zone would impede the analysis of the run in question.

4.6 Computation of Physiological Indices

Subsequently to the identification of the different zones and points of interest in the pressure curves, several indices were computed with the aim of obtaining a correlation between this indices and the indices normally used in clinical practice - iFR and cFFR.

4.6.1 Commonly used Indicators

Instantaneous Wave-Free Ratio

iFR was computed, accordingly to its definition [9], as the mean ratio between the mean distal pressure and the mean aortic pressure, both computed during the WFP (Equation 3.3).

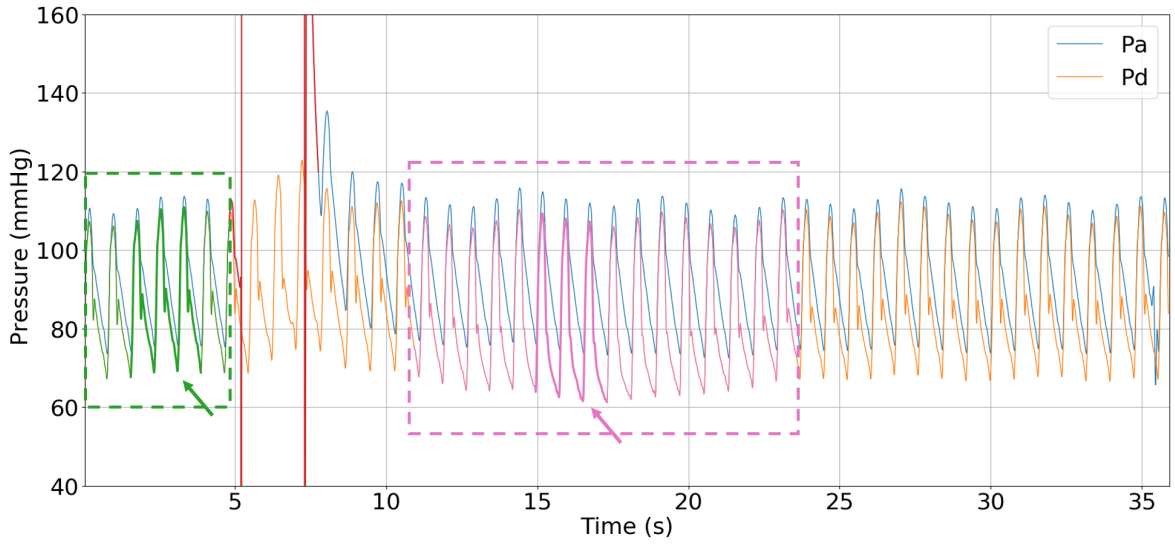

Figure 4.6: Identification of resting, hyperaemic and injection zones. Distal pressure curve (Pd) in blue. Aortic pressure curve (Pa) in orange. Resting zone within green rectangle and resting cycles (**green** arrow). Hyperaemic zone within pink rectangle and hyperaemic cycles (**pink** arrow). Injection artifact in red. Pressure expressed in mmHg and time expressed in seconds.

Resting Full-Cycle Ratio

RFR was calculated, accordingly to its definition [38], as the lowest ratio between distal and aortic pressure measurements, calculated as a moving average. For this moving average, a 9 points moving average was considered (Equation 3.4).

Contrast Fractional Flow Reserve

cFFR was computed, accordingly to FFR definition, as the ratio between the mean distal pressure and the mean aortic pressure, computed during the three hyperaemic cycles (Equation 3.2).

4.6.2 Index 1

With the hypothesis that the area between aortic and distal pressure curves could have a good correlation with iFR, an index that could measure this feature was computed. This is what we call Index 1.

Therefore, the Index 1 aims to differentiate between the two cases in Figure 4.7

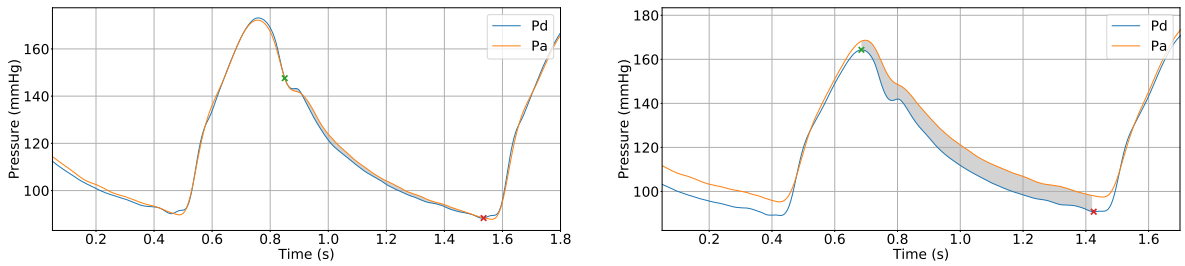

(a) With Pa and Pd interception.

(b) Without Pa and Pd interception.

Figure 4.7: Identification of the area between aortic and distal pressure curves between t_a and t_b. Distal pressure curve (Pd) in blue. Aortic pressure curve (Pa) in orange. Pressure expressed in mmHg and time expressed in seconds.

4.6.3 Index 2

Visual observation of the geometric shape of distal pressure curves, taken from our dataset, led to the formulation of the following hypothesis: Is increasing stenotic severity correlated with increasingly steepest pressure decrease?

In order to test this hypothesis, Index 2 was computed.

4.6.4 Index 3

A simpler index to verify the hypothesis of steepest pressure decrease, in the case of more severe stenosis, was also considered. It consists of the Index 3, computed as a ratio during Period 3. It was hypothesised that in negative cases, i.e. non-significant lesions, Index 3 should be closer to one.

A variation of this index considering Period 1 instead was also computed. In cFFR runs this index was computed considering only the resting cycles or only the hyperaemic cycles.

4.6.5 Index 4

By a visual analysis of several iFR runs, it was hypothesised that the maximum of the geometric measure B on the Period 3 of the curve would reflect a concavity, analogous to the so called curve ventricularization seen in significant lesions, and hence have a correlation with iFR value. Therefore, this index was computed, using the geometric measure B during Period 3. This index was obtained for both distal and aortic pressure curves in order to detect a possible relation between this index before and after the stenosis and the indices obtained in the catheterization lab as is the case of iFR or cFFR.

4.6.6 Indices 5 and 6

As mentioned above, the geometry shape of a pressure curve can be understood through geometric measures B and C. In an attempt to find possible relations between these measures, with both iFR and cFFR, several indices were analysed, at different moments of the cardiac cycle.

Therefore, the mean distal and aortic pressure geometric measures during each of the zones delimited in the cardiac cycle, mentioned above, were computed. Subsequently, the values on Period 2 and 3 were compared. This was performed in order to detect the differences of pressure along the stenosis. In the case of cFFR runs, hyperaemic and resting cycles where treated separately.

4.6.7 Regularization method 2

Despite the application of the regularization method 1 as mentioned above, some small oscillations still persist after using method 1. Such oscillations propagate in the computations, therefore affecting the results.

With the aim of eliminating this small oscillations, Periods 2 and 3 of the each cardiac cycle of the distal and aortic pressure curves were regularized using what we call method 2.

The Indices 3, 5 and 6 were then computed now using the regularized zones.

4.7 Statistical Analysis

With the aim of validating the software developed throughout this thesis and to correlate the new indices developed with the indices usually used in the cath lab, a statistical analysis was performed.

The software was validated thought the comparison of the iFR, RFR and cFFR values obtained, for each run, using the software and the ones measured by the proprietary software in the cath lab. The relationship between indices was quantified by the application of a linear regression and subsequent determination of the correlation coefficient, r^2.

The relationship between the new indices and iFR, RFR or cFFR values was obtained using a linear regression and determining its respective correlation coefficient. The accuracy of the test was measured, using the Receiver Operating Characteristic (ROC) curve, by the calculation of the Area Under the Curve (AUC). The AUC measures the probability that the classifier will rank a randomly chosen positive example higher than a randomly chosen negative example. This statistical method enabled the identification of each index optimal cutoff corresponding to iFR and RFR ≤ 0.89 or to cFFR ≤ 0.83. The ROC curve is a graphical representation of the sensibility (Equation 4.3) against 1 - specificity (Equation 4.4) for each possible cutoff value of a test. The sensitivity and specificity of a test are defined as the probability of a positive or negative example being correctly identified, respectively [45].

The performance of each index in predicting a positive iFR, RFR or cFFR was assessed by Positive Predictive Value (PPV) (Equation 4.1), Negative Predictive Value (NPV) (Equation 4.2), sensitivity (Se) and specificity (Sp) using the cutoff chosen. The optimal cutoff was computed as the point where the Youden's Index (Equation 4.5) was maximal.

$$PPV = \frac{TP}{TP + FP} \tag{4.1}$$

$$NPV = \frac{TN}{TN + FN} \tag{4.2}$$

$$Se = TPR = \frac{TP}{TP + FN} \tag{4.3}$$

$$Sp = 1 - FPR = \frac{TN}{TN + FP} \tag{4.4}$$

$$YI = Se + Sp - 1 \tag{4.5}$$

where,

TP Corresponds to the number of true positives.

TN Represents the number of true negatives.

FP Is to the number of false positives.

FN Represents the number of false negatives.

TPR Corresponds to the true positive rate.

FPR Corresponds to the false positive rate.

5

Validation of the Software

Contents

A first step before introducing the results for the calculation of the various indices described in Chapter 4, is to validate the implemented algorithms, confirming that they are able to compute the indices used in clinical practice. Hence, a comparison between iFR, RFR and cFFR values obtained by the software in HESE and the ones computed in this work was performed and is presented in this chapter.

5.1 Instantaneous Wave-Free Ratio

The iFR values obtained from Philips machine and the results obtained for iFR using this new software were compared. The analysis of Figure 5.1, depicting the linear correlation line from the relation between both iFR values (from the software available in HESE and from the new software developed), shows a very significant correlation ($r^2 = 0.991$) between these two indices.

The small variations to the linear regression line, exhibited in Figure 5.1, may be explained by small differences in the calculus of the location of the dicrotic notch along with variations in the detection of the end of the WFP that are not explicit in the work of Sen *et al.* [9]. Despite that, the strong correlation obtained validates the methodology followed in the computation of the iFR index.

5.2 Resting Full-Cycle Ratio

As referred in Chapter 4, the software from Abbott makes use of a resting index different from iFR, the RFR. Therefore, the same analysis was performed as for iFR, correlating the RFR values computed by the machine at HESE and the RFR values calculated using the present software.

The linear regression analysis, depicted in Figure 5.2, shows a very significant correlation ($y = 1.07x - 0.0819$; $r^2 = 0.973$) between the two measurements. The small deviations to the RFR values obtained in the catheterization laboratory present in Figure 5.2 are caused by variations in the calculation of this index. This index is computed as the lowest ratio between distal and aortic pressures during an entire cycle, calculated as a moving average. Thus, differences in the number of points considered for the calculation of this moving average will cause variations in the measures.

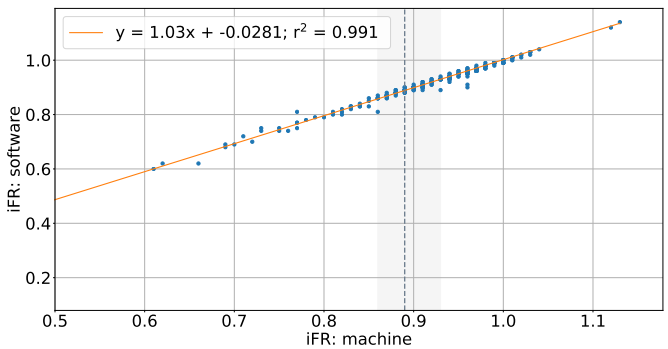

Figure 5.1: Linear correlation between iFR values computed by the proprietary software and the ones calculated using the software developed in this work. Dashed line indicates the cutoff value of 0.89 (in grey) for iFR considered in clinical practice.

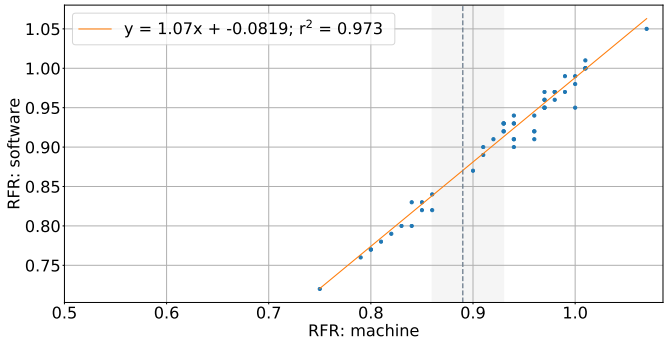

Figure 5.2: Linear correlation between RFR values computed by the proprietary software and the ones calculated using the software developed in this work. Dashed line indicates the cutoff value of 0.89 (in grey) for RFR considered in clinical practice.

5.3 Contrast Fractional Flow Reserve

The determination of the hyperaemic cycles considered into the calculation of cFFR frequently represents a challenge for the software available in clinical practice. Due to the existence of the injection artifact that induces the software to error, the software often fails on the location of these cycles. The cFFR values are then frequently deviated from the correct values and need revision from a cardiologist that detects the error and selects, manually, the location where the cFFR should have been computed. As a consequence, the correlation between cFFR values computed by the proprietary software and the ones manually measured by selecting, manually, the hyperaemic region presents some disagreements.

In order to demonstrate this issue, a linear correlation was applied comparing the values obtained manually and the ones computed by the software in the cath lab. The relation obtained and depicted in Figure 5.3 shows a moderate correlation ($y = 0.894x + 0.0692$; $r^2 = 0.512$) between cFFR measured manually and by the machine, illustrating the disagreements referred above.

The cFFR values computed by the software (Equation 3.2) developed in this thesis were also compared to cFFR values from the manual measurements using the software available at HESE. The linear correlation between these two quantities is exhibited in Figure 5.4.

A very significant correlation ($y = 0.967x + 0.0364$; $r^2 = 0.993$) was obtained with the cFFR computed

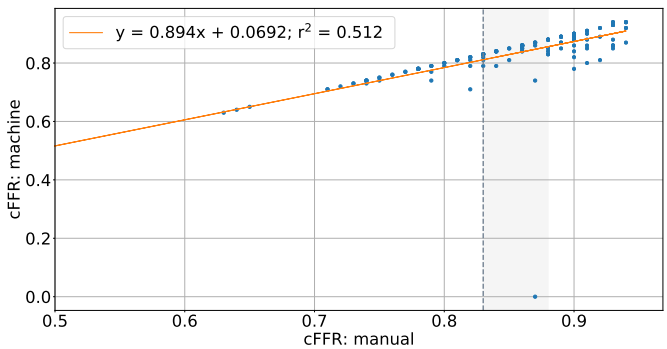

Figure 5.3: Linear correlation between cFFR values computed by the proprietary software and revised by a cardiologist and the ones with no revision. Dashed line indicates the cutoff value of 0.83 (in grey) for cFFR considered in clinical practice.

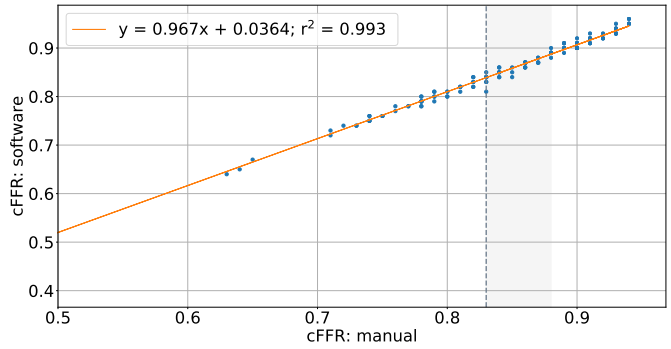

Figure 5.4: Linear correlation between cFFR values computed by the proprietary software and revised by a cardiologist and the ones calculated using the software developed in this work. Dashed line indicates the cutoff value of 0.83 (in grey) for cFFR considered in clinical practice.

by the software having almost no disagreements from the one measured manually. The slight oscillations existing in this correlation could be explained by the way this index is computed by the machine and confirmed by a cardiologist. In the commercial software, cFFR is computed as a moving average of the ratio between distal and aortic pressures, in the more hyperaemic point, where the difference between distal and aortic pressure is maximal. On the other hand, in this work, cFFR is computed as an average of the three more hyperaemic cycles making the measurements potentially less prone to suffer rapid variations and, consequently, to be more robust.

6

Validation of the New Physiological Indices

Contents

The geometrical behaviour of the curves was measured by the different indices already described in Chapter 4. In order to verify the hypothesis behind the computation of each new index, the referred indices were compared to iFR. Thus, 39 iFR runs were chosen from the dataset available. These runs were carefully selected to avoid the inclusion of outliers in this validation. Considering a cutoff value for iFR of 0.89 and a grey zone between 0.86 and 0.93, 13 runs with an iFR value below 0.86 (positive cases), 13 runs with iFR above 0.93 (negative cases) and 13 runs within the grey zone (between 0.86 and 0.93) were considered.

6.1 Index 1

As referred in Chapter 3, van't Veer *et al.* [37] concluded that the various diastolic indices analysed in their study were all identical to iFR. Once the indices considered in that study were computed as the ratio between distal and aortic pressure curves, during different time intervals within the diastolic period, it was expected that the area under the two pressure curves during the same period would be well correlated with iFR.

As depicted in Figure 6.1(a), the Index 1, computed as referred in Chapter 4, is strongly correlated ($y = -0.775x + 0.78$; $r^2 = 0.987$) with iFR obtained in the cath lab. Additionally, the ROC curve exhibited in Figure 6.1(b), calculated using iFR as the reference gold-standard variable and taking a threshold cutoff of 0.89, was found to have an AUC of 99%, suggesting a very high accuracy of the Index 1 as a diagnostic test.

The PPV of this index was 94.4% and the NPV was 95.2%, with a sensitivity and specificity of 94.4% and 95.2%, respectively. This results corroborate the hypothesis that the differences in the down slope of distal and aortic pressure curves are highly correlated with iFR.

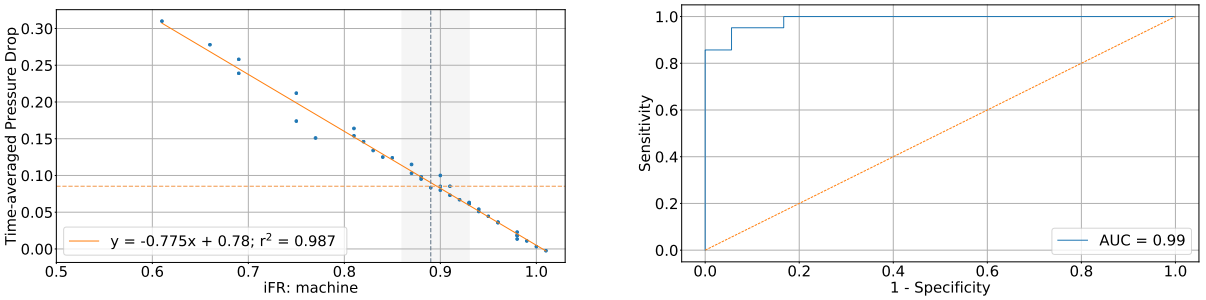

(a) **(b)**

Figure 6.1: **(a)** Linear regression correlating the Index 1 to iFR value. Dashed line in grey indicating the cutoff value considered for iFR (0.89). Light grey shaded area representing iFR grey zone (0.86-0.93). Dashed line in orange indicating the cutoff value computed for the referred index through ROC curve (0.0853). **(b)** ROC curve (in blue) using iFR as the reference gold-standard variable with a threshold cutoff of 0.89.

6.2 Index 2

The correlation between the Index 2 (computed as explicitised in Chapter 4) and iFR, and its diagnostic accuracy to determine the severity of a lesion are presented in Figure 6.2. By the observation of Figure 6.2(a), it is possible to denote a disperse linear correlation between the Index 2 ($y = -0.608x + 0.715$; $r^2 = 0.577$). In spite of this moderate correlation obtained, the ROC curve, exhibited in Figure 6.2(b), calculated using iFR as the reference gold-standard variable and taking a threshold cutoff of 0.89, was found to have an AUC of 84%. This suggests a good accuracy of the Index 1 as a diagnostic test. With the cutoff calculated through ROC curve (0.17), the PPV and NPV were 81.2% and 78.3%, respectively, with a sensitivity of 77.2% and specificity of 85.7%.

This results confirm the hypothesis that, in more severe stenosis, after the systolic peak, the pressure curve decreases faster to lower values which makes the Index 2 to increase. As it is possible to observe in Figure 6.2(a), higher values correspond to lower iFR values, and consequently, to more severe lesions, and vice versa.

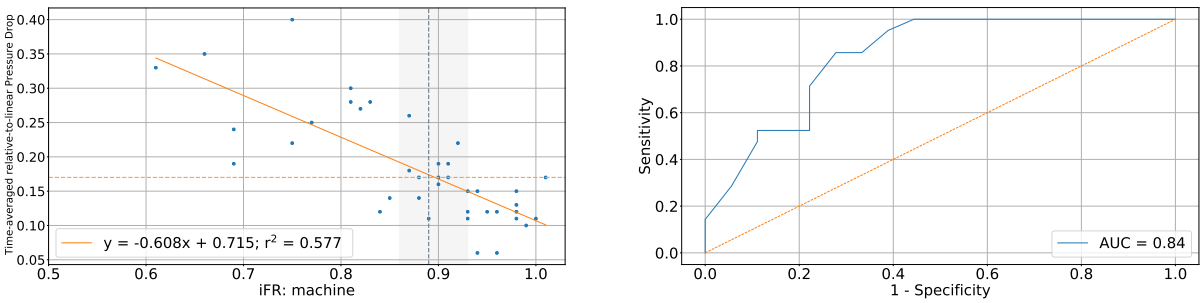

(a) **(b)**

Figure 6.2: **(a)** Linear regression correlating the Index 2 to iFR value. Dashed line in grey indicating the cutoff value considered for iFR (0.89). Light grey shaded area representing iFR grey zone (0.86-0.93). Dashed line in orange indicating the cutoff value computed for the referred index through ROC curve (0.17). **(b)** ROC curve (in blue) using iFR as the reference gold-standard variable with a threshold cutoff of 0.89.

6.3 Index 3

The Index 3 indicator was thought in order to detect the differences existing, between non-significant and significant lesions runs, in the geometric measure C of the Period 1 of the pressure curve. The hypothesis that more severe stenosis would make distal pressure to decrease faster after the systolic peak and, consequently, reach lower values faster than non significant lesions was then formulated. This characteristic would cause the slope in the first quarter of the second part to be negatively higher than the slope in the last quarter of the second part to be almost zero. On the other hand, in a non significant lesion, the slope would not change that much throughout this part of the pressure curve.

The relation between the Index 3 and iFR and its diagnostic accuracy are displayed in Figure 6.3. A moderate correlation between the Index 3 and iFR ($y = 0.935x - 0.584$; $r^2 = 0.453$) was obtained. However, the AUC of the ROC curve shows a good accuracy (AUC = 0.88) of this index in determining

the severity of a stenosis. A PPV of 76.2% and a NPV of 88.9% were obtained with a sensitivity of 88.9% and a specificity of 76.2% considering a cutoff value of 0.24.

With the aim of improving the correlation between Index 3 and iFR, avoiding the bias introduced by the oscillations existent in the derivatives, a variation to this index was proposed. After approximating the second part of the curve to a polynomial of up to fourth order, the Index 3 was computed using that approximation.

The relationship between this new index and the iFR and its diagnosis potential are depicted in Figure 6.4. The linear correlation ($y = 1.06X - 0.713$; $r^2 = 0.441$) and the diagnostic accuracy (AUC = 0.89) obtained show little differences in comparison with the Index 3 computed previously (Figure 6.3(a)). This observation suggests that the small oscillations present in the second part of the curve do not have a major influence on the Index 3.

With the observation that the biggest changes in concavity could be out of the second part of the curve where this index was computed, other variation to the Index 3 index was proposed. This new index, the Index 3, was computed considering the Period 1, starting in the onset of Period 2 and ending

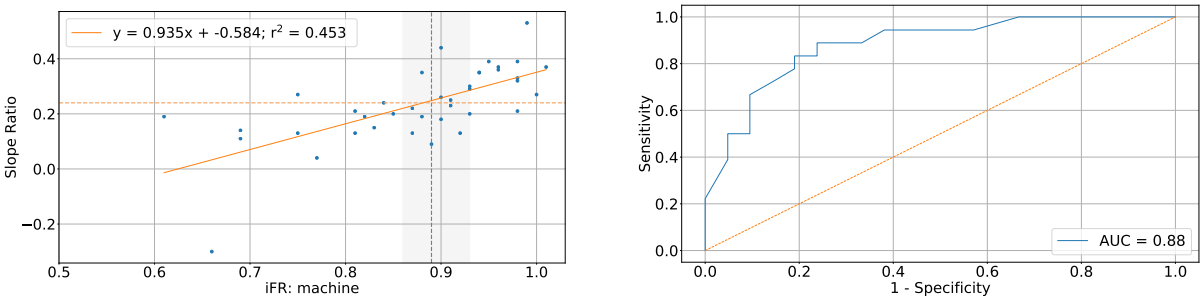

(a) **(b)**

Figure 6.3: **(a)** Linear regression correlating Index 3 to iFR value. Dashed line in grey indicating the cutoff value considered for iFR (0.89). Light grey shaded area representing iFR grey zone (0.86-0.93). Dashed line in orange indicating the cutoff value computed for the referred index through ROC curve (0.24). **(b)** ROC curve (in blue) using iFR as the reference gold-standard variable with a threshold cutoff of 0.89.

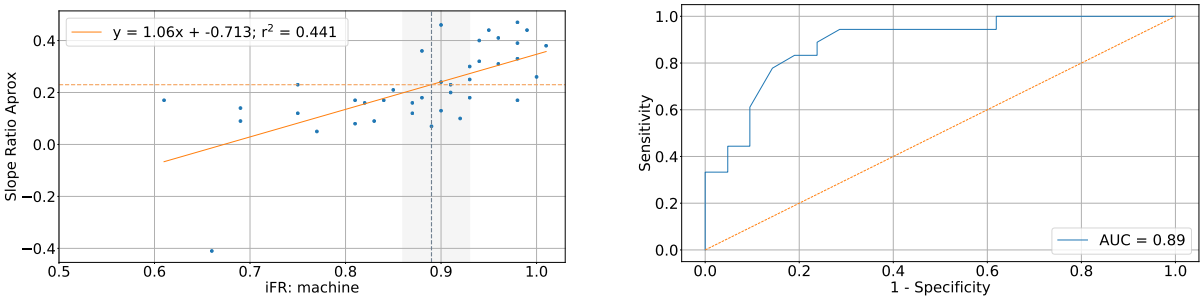

(a) **(b)**

Figure 6.4: **(a)** Linear regression correlating Index 3, measured using regularization method 2 to the second part of the curve, to iFR value. Dashed line in grey indicating the cutoff value considered for iFR (0.89). Light grey shaded area representing iFR grey zone (0.86-0.93). Dashed line in orange indicating the cutoff value computed for the referred index through ROC curve (0.23). **(b)** ROC curve (in blue) using iFR as the reference gold-standard variable with a threshold cutoff of 0.89.

in the end of Period 3. The results for the linear correlation ($y = 0.632X - 0.402$; $r^2 = 0.572$) and the diagnostic accuracy (AUC = 0.91) of this index are presented in Figure 6.5.

A AUC of 0.91 suggests a good diagnostic accuracy of the Index 7 in classify a stenosis in significant or non-significant. Considering a cutoff value of 0.15, a PPV of 85.0% and a NPV of 94.7% were obtained with a sensitivity of 94.4% and a specificity of 85.7%.

Comparing the results obtained for the Index 3 and its variations, it can be stated that the Index 3 considering the entire Period 1 presented the best correlation with iFR and a better diagnostic accuracy in determining whether a lesion is significant or non-significant.

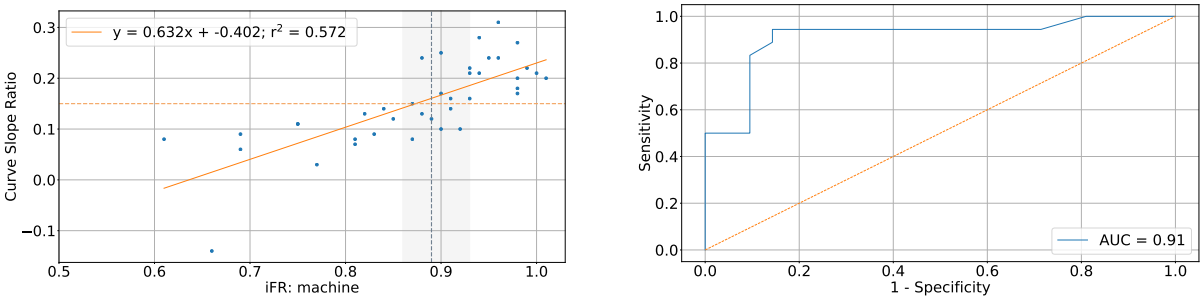

(a) **(b)**

Figure 6.5: **(a)** Linear regression correlating Index 7, measured considering the descending part of the curve, to iFR value. Dashed line in grey indicating the cutoff value considered for iFR (0.89). Light grey shaded area representing iFR grey zone (0.86-0.93). Dashed line in orange indicating the cutoff value computed for the referred index through ROC curve (0.15). **(b)** ROC curve (in blue) iFR as the reference gold-standard variable with a threshold cutoff of 0.89.

6.4 Index 4

In order to test the hypothesis, formulated in the previous chapter (Chapter 4), that the Index 4 would have a correlation with iFR, these two variables were compared. From this comparison, a moderate linear correlation ($y = -7790x + 10600$; $r^2 = 0.393$) was found (Figure 6.6(a)). Despite the relatively low correlation coefficient obtained, it is possible to denote a tendency in this relation where higher peak values correspond to lower iFR values and, consequently, to more significant lesions. Therefore, this suggests that more severe lesions present, normally, a higher curvature in the second part of the curve that can be quantified by the value of the peak.

On the other hand, an AUC of the ROC curve (Figure 6.6(b)) of 0.87 suggests a good diagnostic accuracy of this index. From the ROC curve it was also possible to determine the cutoff value that would maximize the Youden Index. Considering a cutoff of 3300 in this dataset of 39 runs, a PPV of 76.2% and a NPV of 88.9% were obtained with a sensitivity of 88.9% and a specificity of 76.2%.

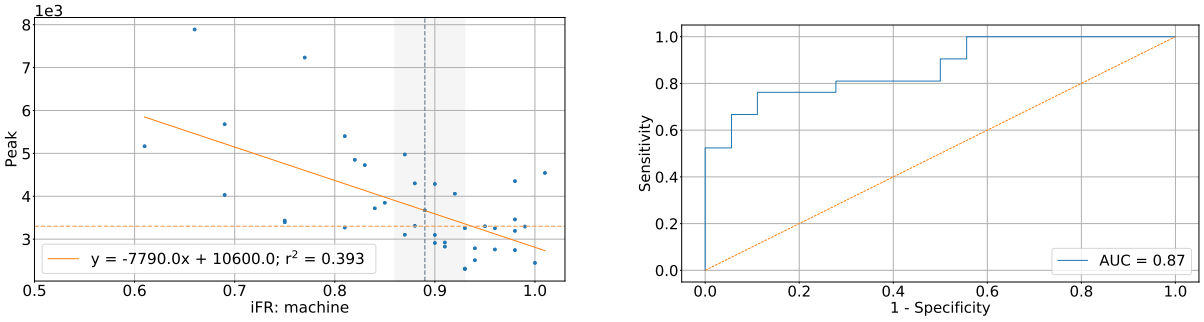

(a) **(b)**

Figure 6.6: **(a)** Linear regression correlating the Index 4 to iFR value. Dashed line in grey indicating the cutoff value considered for iFR (0.89). Light grey shaded area representing iFR grey zone (0.86-0.93). Dashed line in orange indicating the cutoff value computed for the referred index through ROC curve (3300). **(b)** ROC curve (in blue) using iFR as the reference gold-standard variable with a threshold cutoff of 0.89.

6.5 Indices 5 and 6

With the aim of finding a relationship between the slope and concavity of the first and second parts of the curve and the severity of a lesion, ratios between these two parts of the curve were obtained for the geometric measures B and C. The results of these correlations are presented below.

6.5.1 Index 5

The ratio between the second and the Period 2 for the geometric measure C and its correspondent iFR values are represented in Figure 6.7(a). This representation shows very weak correlation between these two indices ($y = 0.115x + 0.0851$; $r^2 = 0.0509$) indicating that there is no relation between this index and iFR. Additionally, the ROC curve analysis (Figure 6.7(b)) also suggests that this index presents a very low diagnostic accuracy (AUC = 0.54).

6.5.2 Index 6

On the other hand, the comparison of the ratio between the second and the Period 2 for the geometric measure B with iFR shows a moderate correlation ($y = -0.562x + 0.589$; $r^2 = 0.331$). However, this relation, represented in Figure 6.7(c), shows a tendency where higher ratios of the geometric measure B correspond to lower values of iFR. This tendency supports the hypothesis that the variation in curvature of the distal pressure curve is correlated with the severity of the lesion.

An analysis of the ROC curve (Figure 6.7(d)) suggests a good accuracy of this ratio in determining whether a lesion is significant or not, presenting an AUC of 0.87. A PPV of 86.7% and a NPV of 79.2% were obtained with a sensitivity of 72.2% and a specificity of 90.5%. This values were calculated using a cutoff value of 0.0818.

6.6 Regularization method 2

In order to overcome the possible errors introduced in the calculation of the indices presented above by the small oscillations existing in the pressure curves, a different regularization method was applied to the curves. The indices were then computed now using the regularization method 2. The results for this new index, regarding geometric measures B and C, are presented and discussed below.

6.6.1 Index 5

The relation between the ratio between Period 3 the Period 2 of the approximated geometric measure C and iFR are presented in Figure 6.7(e). No correlation was found between this two variables ($y = 0.155x + 0.0597$; $r^2 = 0.0779$) reinforcing the results obtained in Section 6.5.1. The analysis of the ROC curve (Figure 6.7(f)) also corroborates this statement once no diagnostic accuracy was found for this index (AUC = 0.59).

6.6.2 Index 6

On the other hand, a moderate correlation ($y = -0.817x + 0.822$; $r^2 = 0.403$) was obtained when comparing the ratios between Period 3 the Period 2 of the approximated geometric measure C and the iFR values (Figure 6.7(g)).

The AUC of the ROC curve of 0.91 was obtained for this new index indicating a significant diagnostic accuracy (Figure 6.7(h)). A cutoff of 0.0786 was computed recurring to the ROC curve. Using this cutoff value, a PPV of 93.3% and a NPV of 83.3% were obtained with a sensitivity and specificity of 77.8% and 95.2%, respectively.

These results suggest that the variation in curvature existent between the first and the second parts of the distal pressure curve constitutes a reasonably good indicator of the severity of a lesion. Moreover, the calculation of the Index 6, using the approximation of the second part of the distal pressure curve by a polynomial, proved to correlate slightly better with iFR than the Index 6 without approximation.

6.7 Summary

From the correlations obtained in this chapter for a selected dataset of 39 runs, it is possible to select some indices that appear to be better correlated with the severity of a lesion.

The Index 1 is closely correlated to iFR value. However, this was already expected once this index measures the difference between both curves, just like iFR. On the other hand, the correlations obtained for the Index 2, the Index 3, the Index 4 and the Index 6 suggest a correlation between the geometry of the distal pressure curve and iFR value.

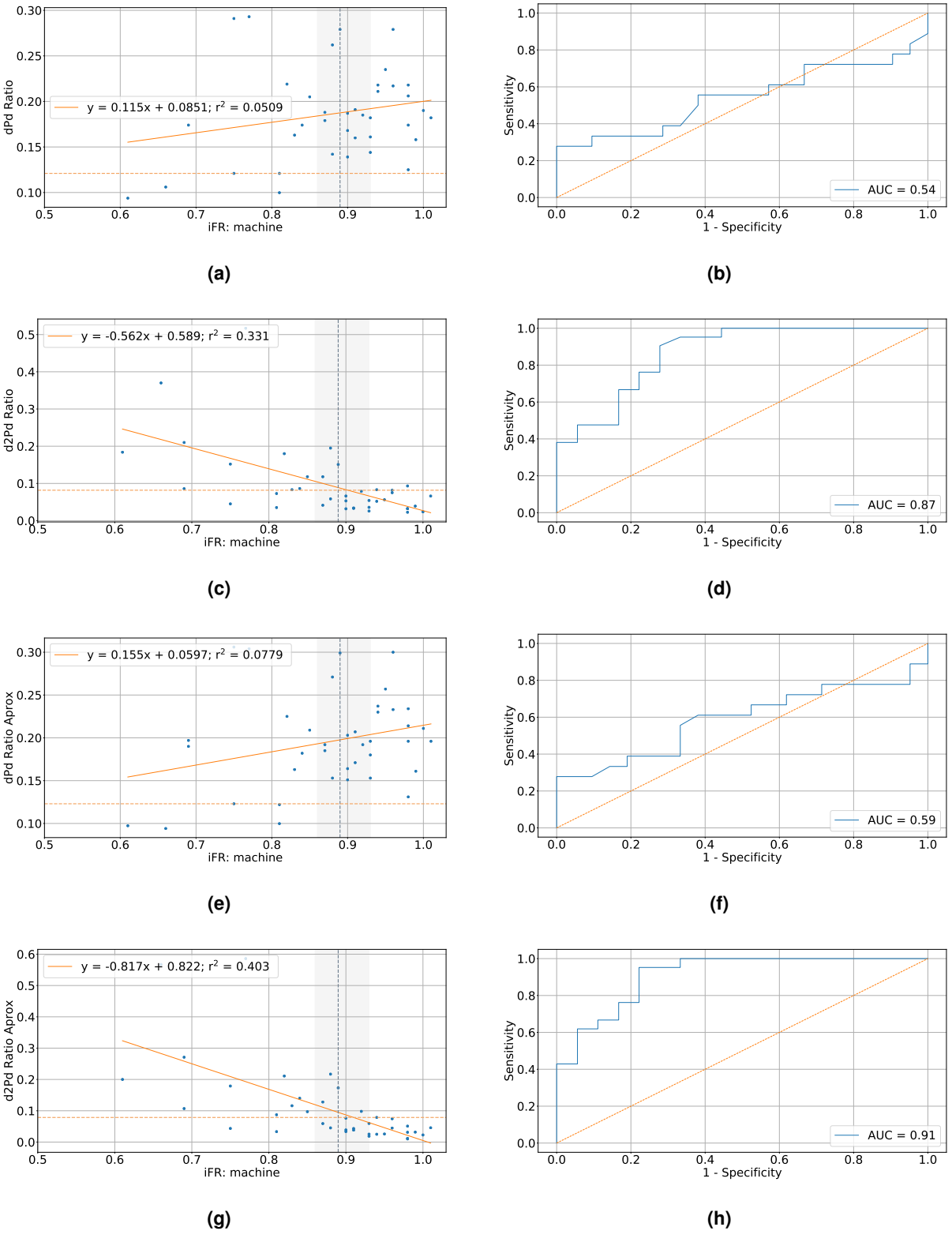

Figure 6.7: Linear regression (left) correlating the ratio between the first and second parts of the pressure curve derivatives to iFR value. ROC curve (right) using iFR as the reference gold-standard variable with a threshold cutoff of 0.89. **(a),(b):** Index 5. **(c),(d):** Index 6. **(e),(f):** Regularization method 2, Index 5. **(g),(h):** Regularization method 2 Index 6. Dashed line in grey indicating the cutoff value considered for iFR (0.89). Light grey shaded area representing iFR grey zone (0.86-0.93). Dashed line in orange indicating the cutoff value computed for the referred index through ROC curve.

7

Results and Discussion

Contents

In this chapter, after the validation of the software developed and of the various new indices designed throughout this thesis, the results for the relationship existent between those indices and iFR and cFFR will be presented considering all runs of the dataset.

7.1 Instantaneous Wave-Free Ratio Runs

In this section, the indices that presented the better correlations with iFR in the previous chapter (Chapter 6), will be compared to iFR, now considering the complete dataset. This indices are: the Index 1, the Index 2, the Index 7, the Index 4 and the Index 6.

The dataset selected to this analysis excludes runs where either the detection of the dicrotic notch (4 runs) or the delineation of the cycles (17 runs) presented any kind of error due to artifacts such as extrasystoles or atrial fibrillation. Runs where, despite the good detection of the different zones in the curve, distal pressure was bigger than aortic pressure (18 runs) or where atrial fibrillation (21 runs), extrasystoles (3 runs) or other type of artifact (21 runs) were present, were also excluded from this analysis. Therefore, 240 iFR runs were considered in the following analysis.

7.1.1 Index 1

The relation between the indicator that measures the Index 1 and iFR, considering all runs of the dataset, is depicted in Figure 7.1(a). As already expected, a very significant correlation ($y = -0.779 + 0.785$; $r^2 = 0.979$) was obtained between these two indices.

Additionally, an AUC of the ROC curve of 0.99 was obtained (Figure 7.1(b)), corroborating the hypothesis that this indicator has a very high diagnosis accuracy when using iFR as the reference gold-standard method. From this analysis, a cutoff value of 0.0853 was computed corresponding to a PPV of 88.4% and a NPV of 99.0% with a sensitivity of 97.4% and a specificity of 95.3%.

Therefore, the Index 1 seems to be a very good predictor of the severity of a lesion, being closely correlated with iFR. However, some limitations on the use of iFR also persist when using this index.

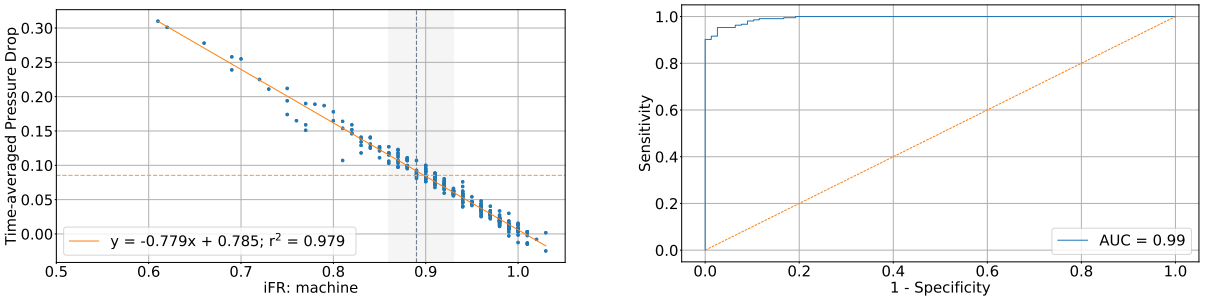

(a) **(b)**

Figure 7.1: **(a)** Linear regression correlating the Index 1 to iFR value. Dashed line in grey indicating the cutoff value considered for iFR (0.89). Light grey shaded area representing iFR grey zone (0.86-0.93). Dashed line in orange indicating the cutoff value computed for the referred index through ROC curve (0.0853). **(b)** ROC curve (in blue) using iFR as the reference gold-standard variable with a threshold cutoff of 0.89.

This is the case of issues such as errors in the equalization of the two pressure sensors, aortic and distal. Thus, other indices that consider only the distal pressure curve will be analysed, despite their lower correlation with iFR.

7.1.2 Distal Pressure Curve

The relations between indices measured, exclusively, using the distal pressure curve and iFR are presented below.

7.1.2.1 Index 2

The comparison between the Index 2 and the iFR values, considering the complete dataset, is exhibited in Figure 7.2. Despite presenting a weak correlation ($y = -0.516x + 0.627$; $r^2 = 0.271$), it is still possible to denote a tendency in Figure 7.2(a) where lower Index 2 values correspond to higher iFR values and, consequently, less significant stenoses. On the other hand, larger areas do not seem to be closely associated with iFR value.

In fact, considering a cutoff value of 0.13, obtained through the ROC curve analysis (Figure 7.2(b)), a NPV of 91.4% was obtained, corroborating that observation. Additionally, the PPV was 42.9% an the NPV was 91.4%. This values correspond to a sensitivity and a specificity of 84.6% and 59.1%, respectively.

7.1.2.2 Index 7

A comparison between the Index 7 and the iFR was obtained considering the complete dataset and is presented in Figure 7.3. From this comparison, a weak correlation was obtained between the two indicators ($y = 0.955x - 0.649$; $r^2 = 0.123$). In spite of this observation, a moderate tendency could be denoted in Figure 7.3(a) where higher Index 7 values seem to correspond to higher values of iFR, although the opposite is not verified.

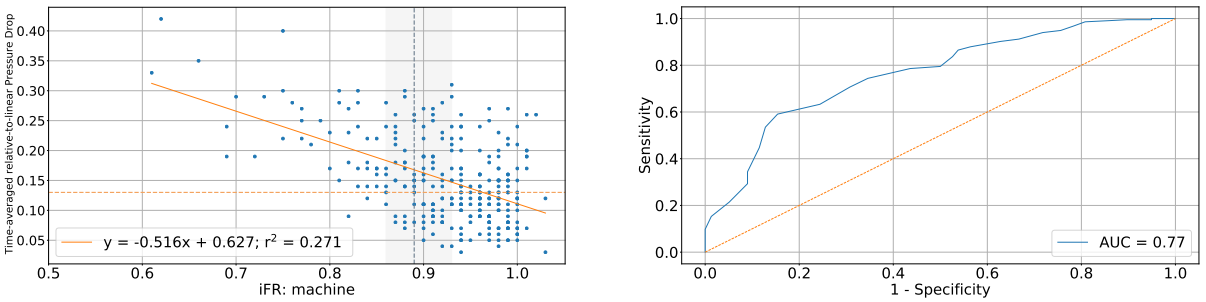

(a) **(b)**

Figure 7.2: **(a)** Linear regression correlating the Index 2 to iFR value. Dashed line in grey indicating the cutoff value considered for iFR (0.89). Light grey shaded area representing iFR grey zone (0.86-0.93). Dashed line in orange indicating the cutoff value computed for the referred index through ROC curve (0.17). **(b)** ROC curve (in blue) using iFR as the reference gold-standard variable with a threshold cutoff of 0.89.

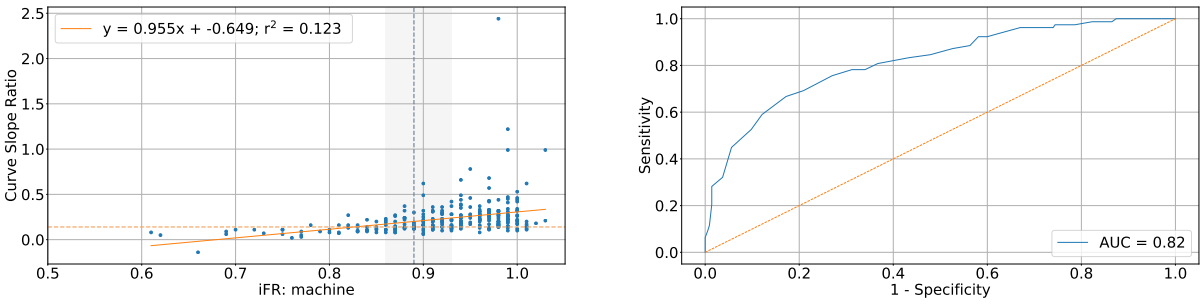

(a) **(b)**

Figure 7.3: (a) Linear regression correlating the Index 7 to iFR value. Dashed line in grey indicating the cutoff value considered for iFR (0.89). Light grey shaded area representing iFR grey zone (0.86-0.93). Dashed line in orange indicating the cutoff value computed for the referred index through ROC curve (0.15). **(b)** ROC curve (in blue) using iFR as the reference gold-standard variable with a threshold cutoff of 0.89.

Supporting this observations, considering a cutoff value of 0.14, computed using the ROC curve (Figure 7.3(b)), a NPV of 87.3% and a PPV of 58.4% were obtained with a sensitivity of 66.7% and a specificity of 82.8%.

7.1.2.3 Index 4

Considering the Index 4, the relationship between this index and iFR is plotted in Figure 7.4(a). A low correlation coefficient was obtained ($y = -7079.0x + 9610.0$; $r^2 = 0.189$) indicating a very weak relation between the Index 4 and iFR.

Additionally, a PPV and a NPV of 41.5% and 87.4% were obtained, respectively, with a sensitivity of 75.6% and a specificity of 61.4%, considering a cutoff value of 2860.

These correlation, lower than the one obtained in Chapter 6, could be explained by the existence of several outliers once the geometric measure B suffers many oscillations in the period were this index is being computed.

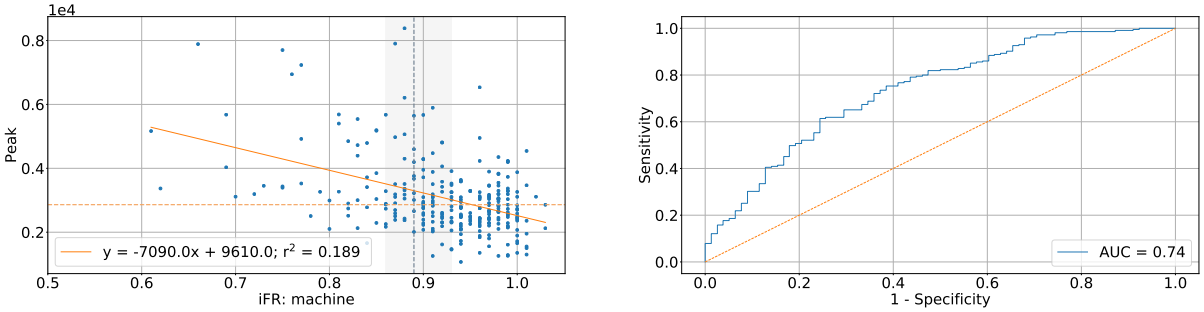

(a) **(b)**

Figure 7.4: (a) Linear regression correlating the the Index 4 to iFR value. Dashed line in grey indicating the cutoff value considered for iFR (0.89). Light grey shaded area representing iFR grey zone (0.86-0.93). Dashed line in orange indicating the cutoff value computed for the referred index through ROC curve (3300). **(b)** ROC curve (in blue) using iFR as the reference gold-standard variable with a threshold cutoff of 0.89.

7.1.2.4 Index 6

Despite presenting a significant diagnostic accuracy (AUC of the ROC curve of 0.82), exhibited in Figure 7.5(b), the correlation obtained between the Index 6 and the iFR value was very weak ($y = -0.796x + 0.802$; $r^2 = 0.0493$). This correlation is depicted in Figure 7.5(a).

A comparison between this result and the one obtained in the previous chapter (Chapter 6) suggests that, probably, the existence of a few outliers in the dataset compromises the tendency verified when considering a more restricted dataset, where higher ratios seem to be associated with lower iFR values and *vice versa*. Considering a cutoff value corresponding to a Index 6 of 0.0547, computed as the maximal Youden Index, a PPV of 60.5% and a NPV of 87.4% were obtained with corresponding sensitivity of 66.7% and a specificity of 84.2%.

7.1.3 Index 7 as an Indicator of Curve Geometry

Regarding the correlations obtained, it is possible to state that the correlation between the Index 1 has a very good correlation with iFR. On the other hand, the relations of the Index 2 and the Index 4 proved to be weaker than the relations obtained in Chapter 6. Despite that, a tendency seems to persist where lower Index 2 and lower peak values correspond to higher iFR. Regarding the Index 6, no relation seems to occur when the 240 iFR runs were considered, possibly due to the existence of a few outliers that could be influencing the correlation. In contrast, a good tendency seems to persist for the Index 7 index. The relation obtained between the Index 7 and iFR suggests that higher Index 7s correspond to higher iFR values and *vice versa*. This index will be used in the next sections as an example of an indicator of the curve geometry.

7.1.4 Influence of Hypotension on Pressure Curve Geometry

While analysing several iFR runs, it was hypothesised that patients with hypotension, i.e. patients where the systolic pressure was below 110 mmHg, presented pressure recordings with a, significantly, more

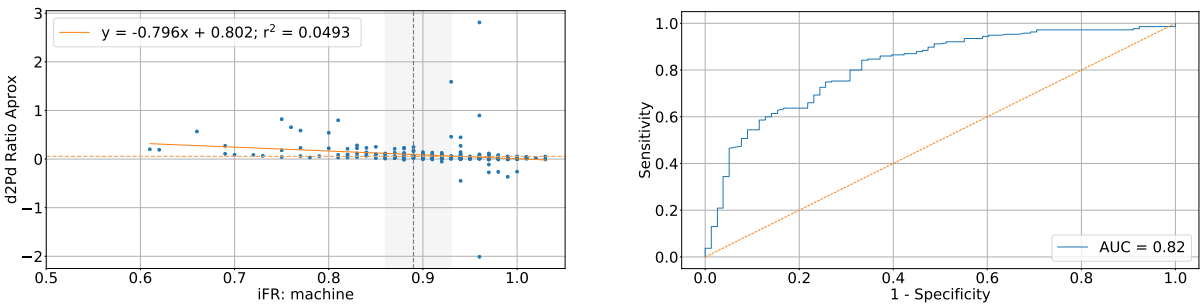

(a) **(b)**

Figure 7.5: **(a)** Linear regression correlating the first and second parts of the curve of the regularized (method 2) geometric measure B to iFR value. Dashed line in grey indicating the cutoff value considered for iFR (0.89). Light grey shaded area representing iFR grey zone (0.86-0.93). Dashed line in orange indicating the cutoff value computed for the referred index through ROC curve (0.0786). **(b)** ROC curve (in blue) using iFR as the reference gold-standard variable with a threshold cutoff of 0.89.

pronounced dicrotic notch. This feature could influence the geometry of the curve and, consequently, influence the calculation of the various parameters measured in this work and its correlation with the indices commonly used in clinical practice, constituting a source of outliers in this correlations.

Therefore, an analysis excluding the 48 runs with systolic pressure below 110 mmHg (measured as the average pressure of the systolic peaks in a run) was performed. The results for the comparison of the Index 7 with iFR, excluding runs with systolic pressure below 110 mmHg, are presented in Figure 7.6. From the ROC curve analysis, a cutoff value of 0.14 was obtained, corresponding to a PPV of 56.5% and a NPV of 86.6% with a sensitivity and a specificity of 68.6% and 79.3%, respectively. These results considering the other indices analysed in Section 7.1 are presented in Appendix B.

The comparison of the correlation depicted in Figure 7.3(a), were the complete dataset is considered, with the correlation presented in Figure 7.6(a), were runs of hypotensive patient were excluded, shows that some outliers that were present in the first are not present when this runs were excluded. This observation suggests that the systolic blood pressure level could have an influence on the geometry of the curve and consequently influence the determination of the indices computed in this thesis.

Therefore, the results presented in the following sections will consider a dataset where these runs where systolic pressure is below 110 mmHg are excluded.

Additionally, the tendency observed in Figure 7.6, where higher Index 7 values correspond to higher values of iFR, suggests that this distal curve geometry indicator could be used as screening test to classify the severity of a coronary lesion. Considering a cutoff value of 0.3 would increase the NPV to 100% which means that all values above these threshold would be negative.

7.1.5 Index 8

Using Index 7 associated with both diastal and aortic pressures, Index 8 was also obtained and compared to iFR. This indicator was computed in an attempt to normalize the Index 7 computed in the distal pressure curve and, consequently, get a curve geometry indicator that would have a better correlation

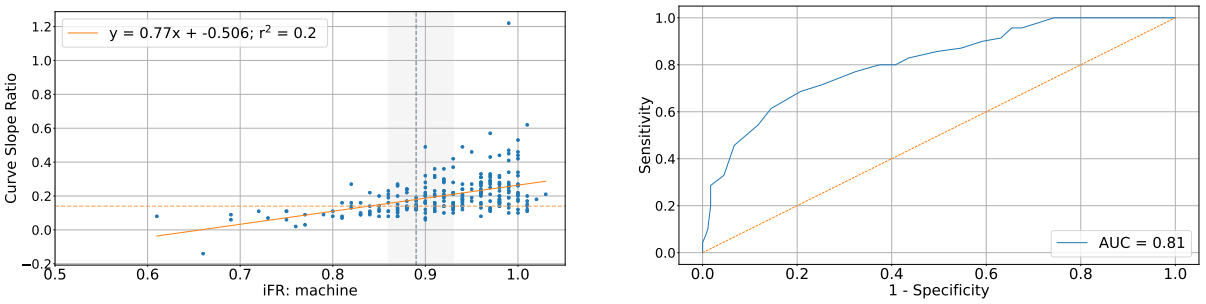

(a) **(b)**

Figure 7.6: **(a)** Linear regression correlating the Index 7 to iFR value considering only runs with systolic pressure above 110 mmHg. Dashed line in grey indicating the cutoff value considered for iFR (0.89). Light grey shaded area representing iFR grey zone (0.86-0.93). Dashed line in orange indicating the cutoff value computed for the referred index through ROC curve (0.14). **(b)** ROC curve (in blue) using iFR as the reference gold-standard variable with a threshold cutoff of 0.89.

with iFR than the ones previously presented in this thesis.

The results obtained are presented in Figure 7.7. A moderate correlation, depicted in Figure 7.7(a) was verified between this indicator and iFR ($y = 2.46x - 1.6$; $r^2 = 0.42$). A tendency where higher Index 7 values correspond to higher iFR values and *vice versa* is also suggested.

An analysis of the ROC curve, exhibited in Figure 7.7(b), shows a good diagnostic accuracy of this indicator in predicting iFR (AUC = 0.84). Considering a cutoff value of 0.649, a PPV of 56.1% and a NPV of 93.0% were obtained with corresponding sensitivity and specificity of 85.7% and 73.7%, respectively.

These results suggest that this indicator, that is based on the geometry of the curve, provides a reasonable alternative to iFR. Additionally, cases where the pressure sensors are not equalized would benefit from this index once it only depends on the shape of the pressure curve and not on the pressure values.

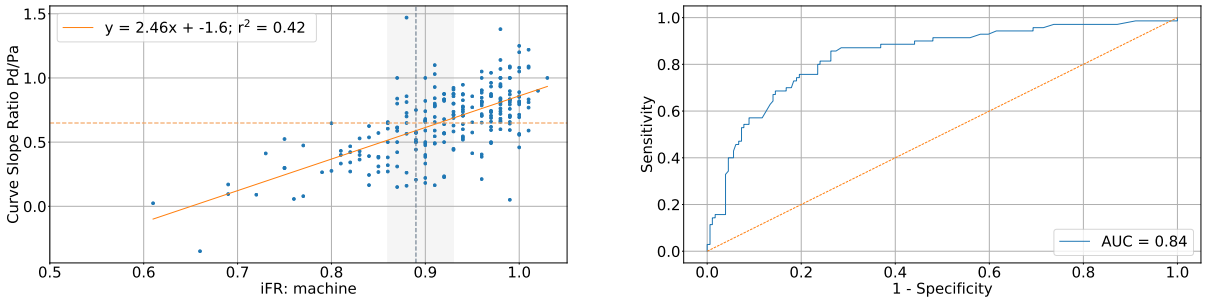

(a) **(b)**

Figure 7.7: **(a)** Linear regression correlating the ratio between distal and aortic pressure curves to iFR value. Dashed line in grey indicating the cutoff value considered for iFR (0.89). Light grey shaded area representing iFR grey zone (0.86-0.93). Dashed line in orange indicating the cutoff value computed for the referred index through ROC curve (0.15). **(b)** ROC curve (in blue) using iFR as the reference gold-standard variable with a threshold cutoff of 0.89.

7.2 Contrast Induced Hyperaemia Runs

After selecting the distal pressure Index 7, measured in the Period 1, a possible indicator of the geometry of the pressure curve, an analysis comparing this indicator with cFFR was performed.

The dataset considered in these analyses excluded runs presenting artifacts such as extrasystoles (5 runs), atrial fibrillation (4 runs) and other artifacts (2 runs), runs with errors in the detection of the cycles (6 runs), in the detection of the dicrotic notch (7 runs) and in the detection of hyperaemic (1 run) or resting regions (2 runs) and runs where the systolic pressure at rest was below 110 mmHg (23 runs). Thus, a total of 129 cFFR runs were analysed.

7.2.1 Contrast Fractional Flow Reserve and Instantaneous Wave-Free Ratio

An iFR value was obtained for cFFR runs computed in the resting cycles. The comparison between this iFR and cFFR, obtained from the proprietary software and reviewed by a cardiologist, is depicted

in Figure 7.8. From this linear regression, a significant correlation was obtained ($y = 0.915x + 0.114$; $r^2 = 0.654$).

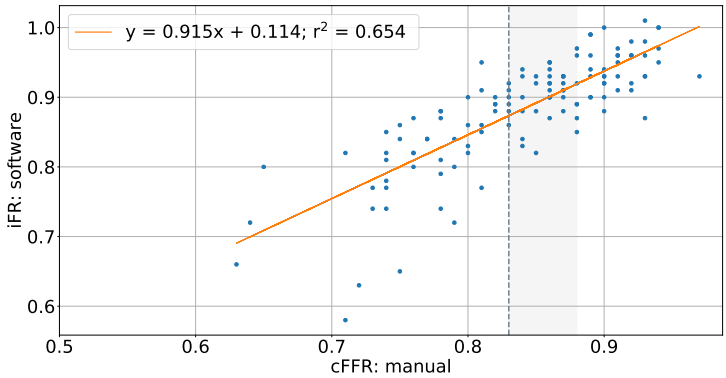

Figure 7.8: Linear correlation between iFR computed in cFFR runs in cycles at rest and cFFR values computed by the proprietary software and revised by a cardiologist. Dashed line in grey indicates the cutoff value of 0.83 for cFFR.

7.2.2 Index 7 for Distal Pressure

In order to verify the relation between distal pressure Index 7 and cFFR, comparisons were obtained for the distal pressure Index 7 measured in the resting cycles (Figure 7.9) and in the cycles under contrast induced hyperaemia (Figure 7.10).

Despite the weak correlations ($y = 0.738x - 0.425$; $r^2 = 0.144$ and $y = 0.604x - 0.412$; $r^2 = 0.205$) obtained in both, resting and hyperaemic, cases, a tendency can be observed where higher Index 7 values correspond to higher cFFR values. This tendency is more evident in the rest case (Figure 7.9(a) and Figure 7.10(a)).

Additionally, the ROC curve analyses performed shows a moderate diagnostic accuracy (AUC = 0.74) for the Index 7 measured at rest when cFFR is considered the reference gold-standard (Figure 7.9(b)). Considering a cutoff value of 0.12, computed as the value that maximizes the Youden Index, a PPV of 73.0% and a NPV of 72.4% were obtained with a sensitivity of 52.9% and a specificity of 86.3%.

From the analysis of Figure 7.9(a) it is possible to state that, using a cutoff value of 0.3, the great majority of the cases classified as negative would be correctly identified, i.e. the NPV would be near 100%. Therefore, with this cutoff value this indicator could be used as screening test. The screening potential of this index was already described in the previous section in Figure 7.6(a), when comparing distal pressure Index 7 with iFR.

Furthermore, the ROC curve analysis performed for the distal pressure Index 7 measured at hyperaemia, considering cFFR as the reference gold-standard method, revealed a good diagnosis accuracy (AUC = 0.81). From this analysis, considering a cutoff value of 0.07, a PPV of 74.4% and a NPV of 76.5% with a sensitivity and a specificity of 62.7% and 84.9%, respectively (Figure 7.10(b)).

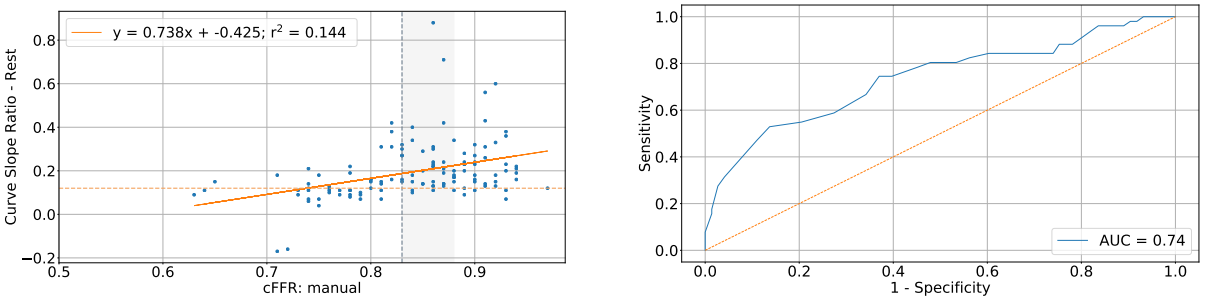

(a) **(b)**

Figure 7.9: **(a)** Linear regression correlating Index 7 measured in the resting cycles to cFFR value. Dashed line in grey indicating the cutoff value considered for cFFR (0.83). Light grey shaded area representing iFR grey zone (0.83-0.88). Dashed line in orange indicating the cutoff value computed for the referred index through ROC curve (0.15). **(b)** ROC curve (in blue) using iFR as the reference gold-standard variable with a threshold cutoff of 0.83.

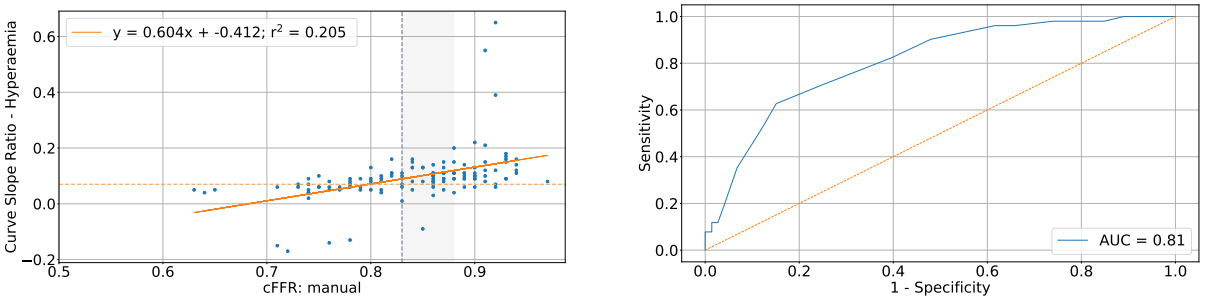

(a) **(b)**

Figure 7.10: **(a)** Linear regression correlating Index 7 measured in the hyperaemic cycles to cFFR value. Dashed line in grey indicating the cutoff value considered for cFFR (0.83). Light grey shaded area representing iFR grey zone (0.83-0.88). Dashed line in orange indicating the cutoff value computed for the referred index through ROC curve (0.15). **(b)** ROC curve (in blue) using iFR as the reference gold-standard variable with a threshold cutoff of 0.83.

7.2.3 Index 8

On the other hand, in order to test the relation between the Index 8 and cFFR, the linear correlation between this two indices was also obtained for both resting and hyperaemic cases. These results are presented in Figure 7.11(a) and in Figure 7.12(a), respectively. A moderate correlation was obtained for both cases ($y = 2.66x - 1.62$; $r^2 = 0.37$ and $y = 2.32x - 1.57$; $r^2 = 0.395$) and are coherent with the ones obtained in the previous section (Figure 7.7(a)) to the comparison to iFR.

The ROC curve computed for the Index 8 measured at rest showed a moderate diagnosis accuracy (AUC = 0.74). A cutoff of 0.583 was obtained corresponding to a PPV of 70.6% and a NPV of 79.5% with a sensitivity of 70.6% and a specificity of 79.5% (Figure 7.11(b)).

Additionally, the ROC curve analysis performed for the ratio between the distal and the aortic pressure Index 7, measured at hyperaemia, suggests that this index presents a significant diagnosis accuracy when considering cFFR as the reference gold standard method (Figure 7.12(b)). Namely, an AUC of the ROC curve of 0.81 was obtained. Moreover, considering a cutoff of 0.357, a PPV of 69.0% and a

NPV of 83.3% were computed, with a sensitivity and a specificity of 78.4% and 75.3%, respectively.

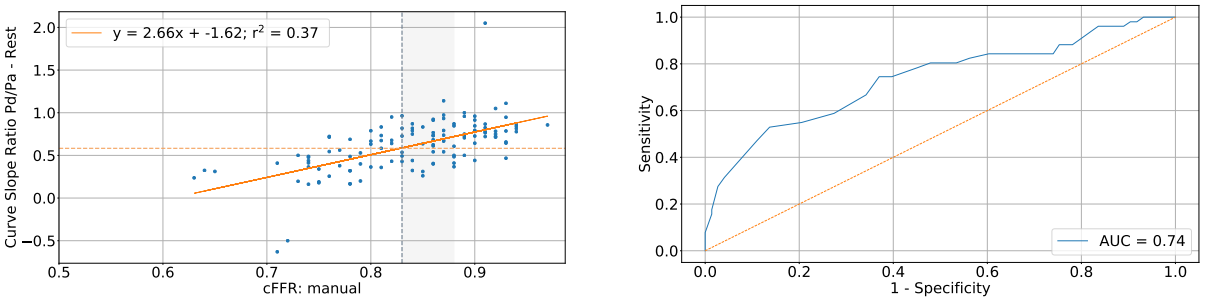

(a) **(b)**

Figure 7.11: **(a)** Linear regression correlating Index 8 measured in the resting cycles to cFFR value. Dashed line in grey indicating the cutoff value considered for cFFR (0.83). Light grey shaded area representing iFR grey zone (0.83-0.88). Dashed line in orange indicating the cutoff value computed for the referred index through ROC curve (0.15). **(b)** ROC curve (in blue) using iFR as the reference gold-standard variable with a threshold cutoff of 0.83.

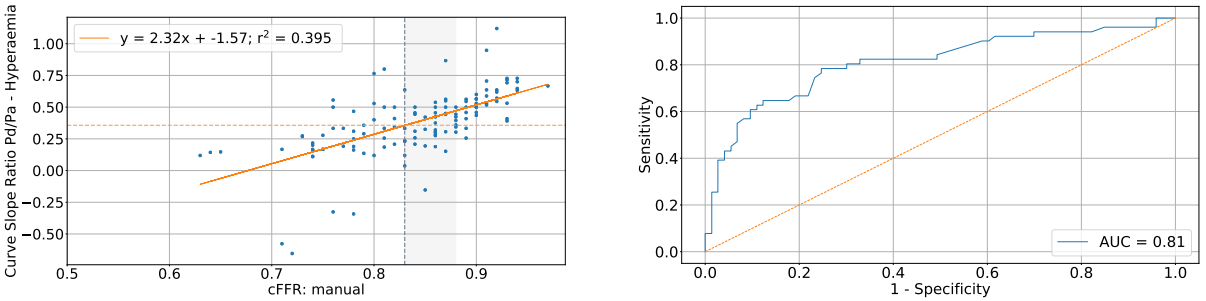

(a) **(b)**

Figure 7.12: **(a)** Linear regression correlating Index 8 measured in the hyperaemic cycles to cFFR value. Dashed line in grey indicating the cutoff value considered for cFFR (0.83). Light grey shaded area representing iFR grey zone (0.83-0.88). Dashed line in orange indicating the cutoff value computed for the referred index through ROC curve (0.15). **(b)** ROC curve (in blue) using iFR as the reference gold-standard variable with a threshold cutoff of 0.83.

7.3 Summary

As a final analysis, some important results were obtained in this thesis.

Firstly, regarding iFR runs, despite presenting moderate to low correlation coefficients, indices as the Index 2 and the Index 7 show a tendency with iFR. While higher Index 2 values appear to be associated with lower iFR values, higher Index 7 values seem to be related to higher iFR values. Therefore, distal pressure curve of more significant stenosis seems to decrease and reach lower values faster after systolic peak than less significant stenosis. These results could suggest that the Index 7 permitted to capture the difference in slopes existing between the first and second parts of the distal pressure curve and the Index 2, allowed a quantification of the concavity of the Period 1 of the distal pressure curve.

On the other hand, indices as the Index 4 and the Index 6, that, using a reduced dataset, showed a

moderate correlation with iFR, enabling a possible quantification of the maximal concavity of the curve during diastole, now showed a poor correlation and no tendency. These differences in results, could be explained by the existence of several outliers in the dataset that influence the correlations. Thus, it is expected that a more rigorous analysis of the dataset, with patient-level fine tuning of the algorithm and eliminating other runs that may have quality anomalies, could lead to a better correlations between this indices and iFR.

From the comparison between results using a complete dataset and results where runs from hypotensive patients were excluded, it was suggested that hypotension could have an influence on the geometry of the pressure curve. This hypothesis was supported by fact that the exclusion of runs presenting a systolic pressure under 110 mmHg showed the removal of some outliers from the relations. This finding was already expected, since the hypotension observed in many patients is induced by fasting ($>$6h by local protocol) administration of nitrates and other drugs during the procedure, thereby provoking a non-physiological state, different from a true basal resting state.

8

Conclusions, Limitations and Future Work

Contents

8.1 Conclusion

In this work several aspects regarding coronary stenosis evaluation with pressure wires were concluded. Firstly, the software developed throughout this thesis proved to have a good correlation with both software used at the catheterization laboratory of HESE, regarding the calculation of traditional indices currently used as a decision tool in clinical practice. Additionally, with respect to the calculation of cFFR, this software have demonstrated to give a reliable and more stable measure of this index.

The relations with iFR of the Index 4, the slope ratio and the Index 2 suggested that the geometrical behaviour of the distal pressure curve is correlated with the severity of coronary lesions, when considering a reduced dataset. Therefore, it seems to be possible to measure lesion severity by analysing pressure curve shape, regardless of its absolute value. This evaluation could be performed by analysing the distal pressure curve only. However, when considering a broader dataset, weaker correlations were obtained.

The Index 7 proved to be a good indicator of the geometry of the curve. Despite not presenting a very significant linear correlation with iFR, a good tendency could be denoted where lesions presenting high Index 7 values would be classified as negative, i.e. non-significant. Additionally, the AUC of the ROC curve suggests a significant, although not perfect, diagnostic accuracy. However, a selection of the correct cutoff value could increase its usefulness as a screening test.

Finally, this study paved the way for a novel method of determining stenosis severity only by the analysis of the pressure recorded distally to the lesion. This would avoid the need of recording aortic pressure and, consequently, avoid possible errors that come from the recording of this pressure as is the case of technical issues such as equalization problems and drift.

8.2 Limitations and Future Work

Due to the great variation existing in dicrotic notch shape among different patients, pathologies and even location of the pressure wire, its detection constituted a challenging step in this work. Even though this problem has been overcome for the most part of the cycles of the runs in the dataset, having obtained a perfect detection, in other cases the detection of this point remained a problem (in less than 3% of the cases). The direct influence that the dicrotic notch location has on the delineation of the different zones in the cardiac cycle together with this detection problem, affects the calculation of indices as is the case of iFR, slope ratio and the different approximations and averages computed in these zones. This limitation could be overcome using a more robust dicrotic notch detection methodology.

On the other hand, the correct detection of the start and end of a cardiac cycle is highly dependent on the initial estimation of the cardiac period. This estimation is computed as an average of the distance between two consecutive systolic peaks. Cardiac cycle alterations by events such as atrial fibrillation or ventricular atrial block that could happen during pressure recordings, affect the cardiac cycle making it considerably larger or smaller in time. These changes may lead to a miscalculation of the initial and final limits of the cycle, influencing all calculations thereafter. A more robust cycle detection that would not

depend on an initial estimation of the cycles length could resolve this limitation.

Moreover, the fact that the number of runs corresponding to more significant lesions available in the dataset were considerably smaller than the number of runs corresponding to non-significant stenosis, could have biased the results.

Additionally, the results obtained in this thesis were compared to either iFR or cFFR acquired in the cath lab, depending on the type of run. However, a comparison with FFR should have also been performed, once the majority of the studies in this field consider FFR as the reference. In a future work, a FFR, a cFFR and a FFR run should be considered for each lesion in order to perform a more robust analysis.

In order to prove the hypothesis that hypotension influences the geometry of the pressure curves, an analysis could be performed where this particular feature would be analysed.

Finally, the relationship between curve pressure shape and lesion severity as assessed by conventional indices is evident in these results. To evaluate the potential of this phenomenon in clinical practice, a clinical study would have to be performed, preferably in a prospective design.

References

[1] P. Libby and P. Theroux, “Pathophysiology of Coronary Artery Disease The Pathophysiology of Chronic CAD,” *Circulation*, vol. 111, pp. 3481–3488, 2005.

[2] “Global Health Estimates 2016: Deaths by Cause, Age, Sex, by Country and by Region, 2000-2016,” Geneva, World Health Organization, 2018.

[3] E. J. Topol and P. S. Teirstein, *Textbook of Interventional Cardiology*, 7th ed. Elsevier, 2016.

[4] M. Roffi, C. Patrono, J. P. Collet, C. Mueller, M. Valgimigli, F. Andreotti, J. J. Bax, M. A. Borger, C. Brotons, D. P. Chew, B. Gencer, G. Hasenfuss, K. Kjeldsen, P. Lancellotti, U. Landmesser, J. Mehilli, D. Mukherjee, R. F. Storey, and S. Windecker, “2015 ESC Guidelines for the management of acute coronary syndromes in patients presenting without persistent st-segment elevation: Task force for the management of acute coronary syndromes in patients presenting without persistent ST-segment elevation,” *European Heart Journal*, vol. 37, no. 3, pp. 273–278, 2016.

[5] S. Shah and S. Pfau, “Coronary Physiology in the Cardiac Catheterization Laboratory,” *Journal of Clinical Medicine*, vol. 8, no. 2, p. 255, feb 2019.

[6] N. H. Pijls, J. A. Van Son, R. L. Kirkeeide, B. De Bruyne, and K. L. Gould, “Experimental basis of determining maximum coronary, myocardial, and collateral blood flow by pressure measurements for assessing functional stenosis severity before and after percutaneous transluminal coronary angioplasty,” *Circulation*, vol. 86, no. 4, pp. 1354–1367, 1993.

[7] J. Knuuti, W. Wijns, A. Saraste, E. Barbato, D. Capodanno, C. Funck-brentano, E. Prescott, R. F. Storey, C. Deaton, T. Cuisset, S. Agewall, K. Dickstein, T. Edvardsen, J. Escaned, B. J. Gersh, P. Svitil, M. Gilard, D. Hasdai, R. Hatala, F. Mahfoud, J. Masip, C. Muneretto, M. Valgimigli, S. Achenbach, and J. J. Bax, “2019 ESC Guidelines for the diagnosis and management of chronic coronary syndromes,” *European Heart Journal*, vol. 00, pp. 7–21, 2019.

[8] J. Z. Lee, N. Singh, I. Nyotowidjojo, C. Howe, S.-W. Low, T. Nguyen, D. Pinto, G. Kumar, and K. S. Lee, “Comparison of regadenoson and nitroprusside to adenosine for measurement of fractional flow reserve: A systematic review and meta-analysis,” *Cardiovascular Revascularization Medicine*, vol. 19, no. 2, pp. 168–174, mar 2018.

[9] S. Sen, J. Escaned, I. S. Malik, G. W. Mikhail, R. A. Foale, R. Mila, J. Tarkin, R. Petraco, C. Broyd, R. Jabbour, A. Sethi, C. S. Baker, M. Bellamy, M. Al-Bustami, D. Hackett, M. Khan, D. Lefroy, K. H.

Parker, A. D. Hughes, D. P. Francis, C. Di Mario, J. Mayet, and J. E. Davies, “Development and Validation of a New Adenosine-Independent Index of Stenosis Severity From Coronary Wave–Intensity Analysis,” *Journal of the American College of Cardiology*, vol. 59, no. 15, pp. 1392–1402, apr 2012.

[10] S. V. Guzman and J. W. West, “Cardiac effects of intracoronary arterial injections of various roentgenographic contrast media,” *American Heart Journal*, vol. 58, no. 4, pp. 597–607, oct 1959.

[11] A. M. Leone, G. Scalone, G. L. De Maria, F. Tagliaferro, A. Gardi, F. Clemente, E. Basile, P. Cialdella, A. R. De Caterina, I. Porto, C. Aurigemma, F. Burzotta, G. Niccoli, C. Trani, A. G. Rebuzzi, and F. Crea, “Efficacy of contrast medium induced Pd/Pa ratio in predicting functional significance of intermediate coronary artery stenosis assessed by fractional flow reserve: insights from the RINASCI study,” *EuroIntervention*, vol. 11, no. 4, pp. 421–427, aug 2015.

[12] B. F. Waller, C. M. Orr, J. D. Slack, C. A. Pinkerton, J. Van Tassel, and T. Peters, “Anatomy, histology, and pathology of coronary arteries: A review relevant to new interventional and imaging techniques-Part I,” *Clinical Cardiology*, vol. 15, no. 7, pp. 451–457, jul 1992.

[13] J. G. Betts, K. A. Young, J. A. Wise, E. Johnson, B. Poe, D. H. Kruse, O. Korol, J. E. Johnson, M. Womble, and P. DeSaix, *Anatomy and Physiology*. Houston, Texas: OpenStax, 2013.

[14] S. Patel, “Normal and Anomalous Anatomy of the Coronary Arteries,” *Seminars in Roentgenology*, vol. 43, no. 2, pp. 100–112, apr 2008.

[15] G. J. Crystal, S. I. Assaad, and P. M. Heerdt, “Cardiovacular System,” in *Pharmacology and Physiology for Anesthesia*, 2nd ed. Elsevier Inc., 2019, ch. 24, pp. 473–519.

[16] T. P. van de Hoef, M. Meuwissen, J. Escaned, J. E. Davies, M. Siebes, J. A. E. Spaan, and J. J. Piek, “Fractional flow reserve as a surrogate for inducible myocardial ischaemia,” *Nature Reviews Cardiology*, vol. 10, no. 8, pp. 439–452, aug 2013.

[17] G. Crystal and L. Klein, “Fractional Flow Reserve: Physiological Basis, Advantages and Limitations, and Potential Gender Differences,” *Current Cardiology Reviews*, vol. 11, no. 3, pp. 209–219, 2015.

[18] K. Lipscomb and K. L. Gould, “Mechanism of the effect of coronary artery stenosis on coronary flow in the dog,” *American Heart Journal*, vol. 89, no. 1, pp. 60–67, 1975.

[19] B. F. Waller, “The eccentric coronary atherosclerotic plaque: Morphologic observations and clinical relevance,” *Clinical Cardiology*, vol. 12, no. 1, pp. 14–20, 1989.

[20] T. Doenst, A. Haverich, P. Serruys, R. O. Bonow, P. Kappetein, V. Falk, E. Velazquez, A. Diegeler, and H. Sigusch, “PCI and CABG for Treating Stable Coronary Artery Disease: JACC Review Topic of the Week,” *Journal of the American College of Cardiology*, vol. 73, no. 8, pp. 964–976, 2019.

[21] “Percutaneous Coronary Intervention — National Heart, Lung, and Blood Institute (NHLBI),” 2011. [Online]. Available: https://www.nhlbi.nih.gov/health-topics/percutaneous-coronary-intervention

[22] “Coronary Artery Bypass Grafting — National Heart, Lung, and Blood Institute (NHLBI),” 2015. [Online]. Available: https://www.nhlbi.nih.gov/health-topics/coronary-artery-bypass-grafting

[23] F.-J. Neumann and M. Sousa-Uva, “2018 ESC/EACTS Guidelines on myocardial revascularization The Task Force on myocardial revascularization of the European Society of Cardiology (ESC) and European Association for Cardio-Thoracic Surgery (EACTS) Developed with the special contribution of th,” *European Heart Journal*, vol. 00, pp. 1–96, 2018.

[24] E. Moniz, “Die Arterielle Encephalographie als Methode zur Lokalisierung von Hirntumoren,” *Klinische Wochenschrift*, vol. 8, no. 24, pp. 1118–1122, 1929.

[25] S. Satheesh and A. Subramanian, “How to do radial coronary angiogram?” pp. 170–174, 2015.

[26] A. J. Klein and P. M. Patel, *3 – Coronary Angiography and Ventriculography*, 6th ed. Elsevier Inc., 2016.

[27] K. L. Gould, K. Lipscomb, and G. W. Hamilton, “Physiologic basis for assessing critical coronary stenosis. Instantaneous flow response and regional distribution during coronary hyperemia as measures of coronary flow reserve,” *The American Journal of Cardiology*, vol. 33, no. 1, pp. 87–94, 1974.

[28] A. M. Leone, F. Lassandro Pepe, M. Arioti, and F. Crea, “Contrast Fractional Flow Reserve (cFFR): A pragmatic response to the call for simplification of invasive functional assessment,” *International Journal of Cardiology*, vol. 268, pp. 45–50, 2018.

[29] Y. Kawase, H. Omori, M. Kawasaki, T. Tanigaki, T. Hirata, S. Okamoto, H. Ota, J. Kikuchi, M. Okubo, H. Kamiya, A. Hirakawa, T. Suzuki, and H. Matsuo, “Postocclusional Hyperemia for Fractional Flow Reserve after Percutaneous Coronary Intervention,” *Circulation: Cardiovascular Interventions*, vol. 10, no. 12, pp. 1–6, 2017.

[30] N. H. Pijls and P. A. Tonino, “The crux of maximum hyperemia: The last remaining barrier for routine use of fractional flow reserve,” pp. 1093–1095, 2011.

[31] J. E. Davies, Z. I. Whinnett, D. P. Francis, C. H. Manisty, J. Aguado-Sierra, K. Willson, R. A. Foale, I. S. Malik, A. D. Hughes, K. H. Parker, and J. Mayet, “Evidence of a dominant backward-propagating ”suction” wave responsible for diastolic coronary filling in humans, attenuated in left ventricular hypertrophy,” *Circulation*, vol. 113, no. 14, pp. 1768–1778, 2006.

[32] J. Escaned, M. Echavarría-Pinto, H. M. Garcia-Garcia, T. P. Van De Hoef, T. De Vries, P. Kaul, G. Raveendran, J. D. Altman, H. I. Kurz, J. Brechtken, M. Tulli, C. Von Birgelen, J. E. Schneider, A. A. Khashaba, A. Jeremias, J. Baucum, R. Moreno, M. Meuwissen, G. Mishkel, R. J. Van Geuns, H. Levite, R. Lopez-Palop, M. Mayhew, P. W. Serruys, H. Samady, J. J. Piek, and A. Lerman, “Prospective assessment of the diagnostic accuracy of instantaneous wave-free ratio to assess coronary stenosis relevance: Results of ADVISE II international, multicenter study (ADenosine

vasodilator independent stenosis evaluation II)," *JACC: Cardiovascular Interventions*, vol. 8, no. 6, pp. 824–833, 2015.

[33] C. Berry, M. Van 'T Veer, N. Witt, P. Kala, O. Bocek, S. A. Pyxaras, J. D. McClure, W. F. Fearon, E. Barbato, P. A. Tonino, B. De Bruyne, N. H. Pijls, and K. G. Oldroyd, "VERIFY (VERification of instantaneous wave-free ratio and fractional flow reserve for the assessment of coronary artery stenosis severity in everyday practice): A multicenter study in consecutive patients," *Journal of the American College of Cardiology*, vol. 61, no. 13, pp. 1421–1427, apr 2013.

[34] A. Jeremias, A. Maehara, P. Généreux, K. N. Asrress, C. Berry, B. De Bruyne, J. E. Davies, J. Escaned, W. F. Fearon, K. L. Gould, N. P. Johnson, A. J. Kirtane, B.-K. Koo, K. M. Marques, S. Nijjer, K. G. Oldroyd, R. Petraco, J. J. Piek, N. H. Pijls, S. Redwood, M. Siebes, J. A. Spaan, M. van 't Veer, G. S. Mintz, and G. W. Stone, "Multicenter Core Laboratory Comparison of the Instantaneous Wave-Free Ratio and Resting P d /P a With Fractional Flow Reserve," *Journal of the American College of Cardiology*, vol. 63, no. 13, pp. 1253–1261, apr 2014.

[35] J. E. Davies, S. Sen, H. M. Dehbi, R. Al-Lamee, R. Petraco, S. S. Nijjer, R. Bhindi, S. J. Lehman, D. Walters, J. Sapontis, L. Janssens, C. J. Vrints, A. Khashaba, M. Laine, E. Van Belle, F. Krackhardt, W. Bojara, O. Going, T. Härle, C. Indolfi, G. Niccoli, F. Ribichini, N. Tanaka, H. Yokoi, H. Takashima, Y. Kikuta, A. Erglis, H. Vinhas, P. Canas Silva, S. B. Baptista, A. Alghamdi, F. Hellig, B. K. Koo, C. W. Nam, E. S. Shin, J. H. Doh, S. Brugaletta, E. Alegria-Barrero, M. Meuwissen, J. J. Piek, N. Van Royen, M. Sezer, C. Di Mario, R. T. Gerber, I. S. Malik, A. S. Sharp, S. Talwar, K. Tang, H. Samady, J. Altman, A. H. Seto, J. Singh, A. Jeremias, H. Matsuo, R. K. Kharbanda, M. R. Patel, P. Serruys, and J. Escaned, "Use of the instantaneous wave-free ratio or fractional flow reserve in PCI," *New England Journal of Medicine*, vol. 376, no. 19, pp. 1824–1834, 2017.

[36] M. Götberg, E. H. Christiansen, I. J. Gudmundsdottir, L. Sandhall, M. Danielewicz, L. Jakobsen, S. E. Olsson, P. Öhagen, H. Olsson, E. Omerovic, F. Calais, P. Lindroos, M. Maeng, T. Tödt, D. Venetsanos, S. K. James, A. Karegren, M. Nilsson, J. Carlsson, D. Hauer, J. Jensen, A. C. Karlsson, G. Panayi, D. Erlinge, and O. Fröbert, "Instantaneous wave-free ratio versus fractional flow reserve to guide PCI," *New England Journal of Medicine*, vol. 376, no. 19, pp. 1813–1823, 2017.

[37] M. van't Veer, N. H. Pijls, B. Hennigan, S. Watkins, Z. A. Ali, B. De Bruyne, F. M. Zimmermann, L. X. van Nunen, E. Barbato, C. Berry, and K. G. Oldroyd, "Comparison of Different Diastolic Resting Indexes to iFR: Are They All Equal?" *Journal of the American College of Cardiology*, vol. 70, no. 25, pp. 3088–3096, 2017.

[38] J. Svanerud, J. M. Ahn, A. Jeremias, M. Van 'T Veer, A. Gore, A. Maehara, A. Crowley, N. H. Pijls, B. De Bruyne, N. P. Johnson, B. Hennigan, S. Watkins, C. Berry, K. G. Oldroyd, S. J. Park, and Z. A. Ali, "Validation of a novel non-hyperaemic index of coronary artery stenosis severity: The Resting Full-cycle Ratio (VALIDATE RFR) study," *EuroIntervention*, vol. 14, no. 7, pp. 806–814, 2018.

[39] B. De Bruyne, N. H. J. Pijls, E. Barbato, J. Bartunek, J. W. Bech, W. Wijns, and G. R. Heyndrickx, "Intracoronary and intravenous adenosine 5′-triphosphate, adenosine, papaverine, and contrast medium to assess fractional flow reserve in humans," *Circulation*, vol. 107, no. 14, pp. 1877–1883, 2003.

[40] N. P. Johnson, A. Jeremias, F. M. Zimmermann, J. Adjedj, N. Witt, B. Hennigan, B.-K. Koo, A. Maehara, M. Matsumura, E. Barbato, G. Esposito, B. Trimarco, G. Rioufol, S.-J. Park, H.-M. Yang, S. B. Baptista, G. S. Chrysant, A. M. Leone, C. Berry, B. De Bruyne, K. L. Gould, R. L. Kirkeeide, K. G. Oldroyd, and N. H. Pijls, "Continuum of Vasodilator Stress From Rest to Contrast Medium to Adenosine Hyperemia for Fractional Flow Reserve Assessment," *JACC: Cardiovascular Interventions*, vol. 9, no. 8, pp. 757–767, 2016.

[41] A. M. Leone, R. Martin-Reyes, S. B. Baptista, N. Amabile, L. Raposo, J. A. Franco Pelaez, C. Trani, P. Cialdella, E. Basile, G. Zimbardo, F. Burzotta, I. Porto, C. Aurigemma, A. G. Rebuzzi, M. Faustino, G. Niccoli, P. F. Abreu, M. S. Slama, V. Spagnoli, M. T. Arrieta, I. J. Amat Santos, J. M. De La Torre Hernandez, R. L. Palop, and F. Crea, "The Multi-center Evaluation of the Accuracy of the Contrast MEdium INduced Pd/Pa RaTiO in Predicting FFR (MEMENTOFFR) Study," *EuroIntervention*, vol. 12, no. 6, pp. 708–715, 2016.

[42] R. J. McGeoch and K. G. Oldroyd, "Pharmacological options for inducing maximal hyperaemia during studies of coronary physiology," *Catheterization and Cardiovascular Interventions*, vol. 71, no. 2, pp. 198–204, 2008.

[43] B. N. Li, M. C. Dong, and M. I. Vai, "On an automatic delineator for arterial blood pressure waveforms," *Biomedical Signal Processing and Control*, vol. 5, no. 1, pp. 76–81, 2010.

[44] M. J. Oppenheim and D. F. Sittig, "An innovative dicrotic notch detection algorithm which combinesrule-based logic with digital signal processing techniques," *Computers and Biomedical Research*, vol. 28, no. 2, pp. 154–170, 1995.

[45] F. Habibzadeh, P. Habibzadeh, and M. Yadollahie, "On determining the most appropriate test cut-off value: The case of tests with continuous results," *Biochemia Medica*, vol. 26, no. 3, pp. 297–307, 2016.

Formulas for geometric measures

Several equations were required for the computation of geometric measures A, B and C. This appendix refers to such equations.

B

Influence of Hypotension on Pressure Curve Geometry

Linear correlations and ROC curve of the Index 1 (Figures B.1(a) and B.1(b)), the Index 2 (Figures B.1(c) and B.1(d)), Index 4 (Figures B.1(e) and B.1(f)) and the ratio between the geometric measure B (regularization method 2) Period 3 the Period 2. (Figures B.1(g) and B.1(h)) with iFR considering a dataset where runs with systolic pressure below 110 mmHg where excluded.

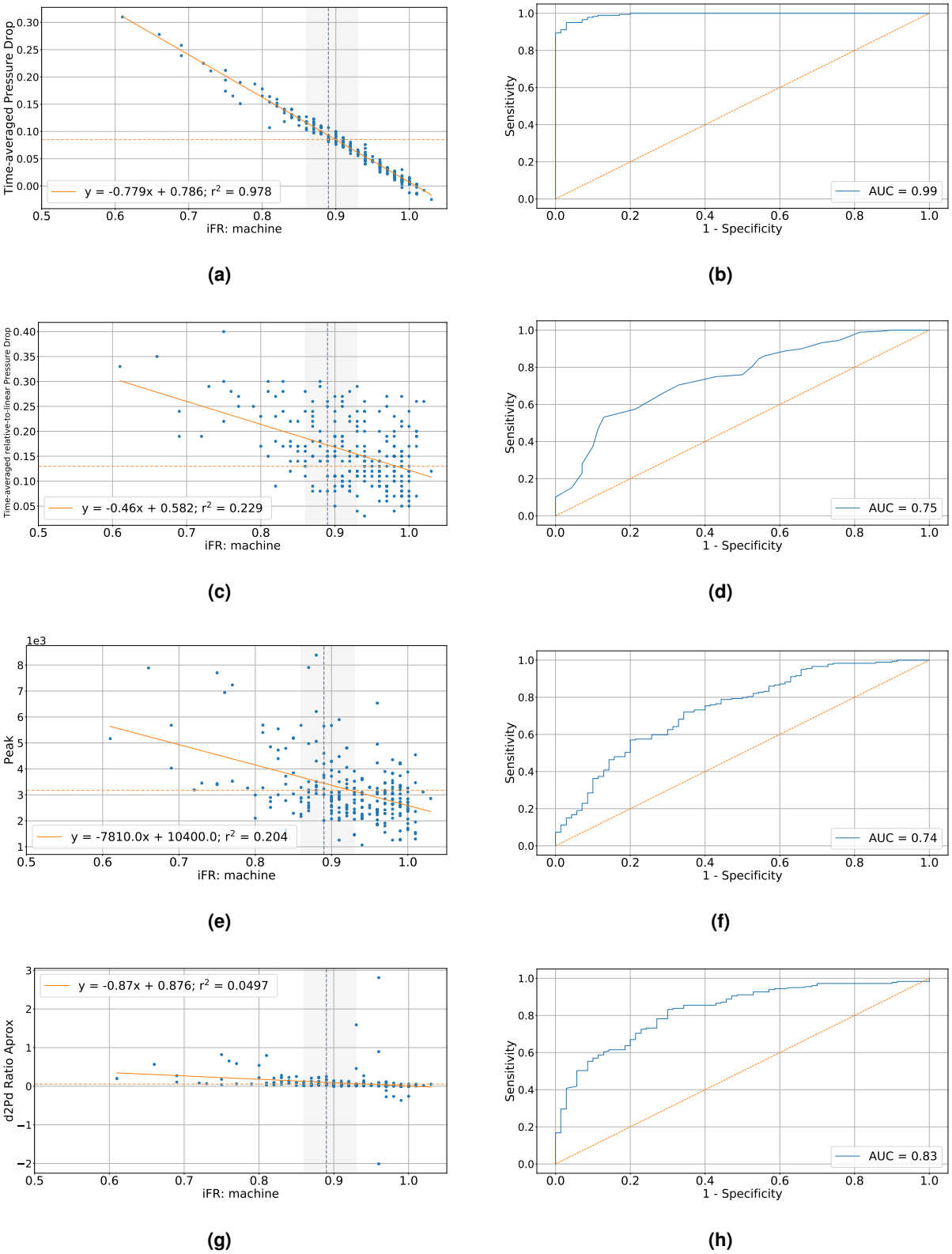

Figure B.1: Linear regression (left) and ROC curve (right in blue) for the new indices using iFR as the reference gold-standard (cutoff = 0.89). **(a),(b):** Index 1 (cutoff = 0.0853). **(c),(d):** Index 2 (cutoff = 0.13). **(e),(f):** Index 4 (cutoff = 3170). **(g),(h):** Index 6 (cutoff = 0.0547). Dashed line in grey indicating the cutoff value considered for iFR (0.89). Light grey shaded area representing iFR grey zone (0.86-0.93). Dashed line in orange indicating the cutoff value computed through ROC curve.